A New Approach of EV Modeling and Its Control Applications to Reduce Energy Consumption

RINA RISTIANA[1], (Student Member, IEEE), **ARIEF SYAICHU ROHMAN**[1], (Member, IEEE),
CARMADI MACHBUB[1], (Member, IEEE), **AGUS PURWADI**[1,2], (Member, IEEE),
AND ESTIKO RIJANTO[3], (Member, IEEE)

[1]School of Electrical Engineering and Informatics, Institut Teknologi Bandung, Bandung 40132, Indonesia
[2]National Centre for Sustainable Transportation Technology, Bandung 40132, Indonesia
[3]Research Centre for Electrical Power and Mechatronics, Indonesian Institute of Sciences, Bandung 40135, Indonesia

Corresponding author: Rina Ristiana (rina005@lipi.go.id)

ABSTRACT Efficient energy usage of electric vehicles (EVs) is an important concern, especially in relation to the use of battery energy. This paper presents a strategy to make the use of battery energy more economical by employing a new modeling approach. One of the existing EV models, called the motor-vehicle model, considers the motor and the longitudinal vehicle dynamics. In this study, the motor-vehicle model is further simplified by ignoring the drag force, which will be referred to as the simple model. In addition, we propose a new approach of EV modeling by including the battery dynamics into a motor-vehicle model and taking into account the drag force. This model is named the Integrated Battery-Electric Vehicle (IBEV) model. In order to demonstrate the usefulness of the proposed model, controllers are designed using linear quadratic integral (LQI) control. Each controller is designed for several test cases based on a linearized integrated model, after which specific test cases are carried out on a nonlinear IBEV model. From these models, the energy consumption is analyzed based on several performance indices under a number of combinations of settings, i.e. battery type (lithium-ion or lead-acid battery) and shaft model (rigid or flexible shaft). Further, an LQI controller with a Kalman filter is designed and its performance is compared to LQI controllers with 4th and 5th order Luenberger observers. The simulation results shows that the use of IBEV model reduces energy consumption compared to the use of simple model in controller design, and that the LQI controller with Kalman filter can reduce the noise effect and is more economical than the controllers with other observers.

INDEX TERMS Electric vehicle, IBEV models, efficient energy usage, LQI control, Kalman filter.

NOMENCLATURE

ω_m	Motor angular speed
T_m	Motor torque
i_m	Motor current
V_b	Battery voltage
V_m	Motor voltage
u_c	Control signal
T_w	Wheel torque
ω_d	Shaft angular speed
i_1	Branch current of lead-acid battery
Q_b	Capacity of lead-acid battery
ω_w	Wheel angular speed
θ_m	Motor position
θ_d	Shaft position
θ_w	Wheel position
i_b	Battery current
K_c	PWM gain
V_{c1}	1st terminal voltage of lithium-ion battery
V_{c2}	2nd terminal voltage of lithium-ion battery
SOC_n	State of charge of lithium-ion
θ_b	Electrolyte temperature of lead-acid battery
EV	Electric vehicle
DOF	Degree of freedom
IBEV	Integrated battery-electric vehicle
HILS	Hardware in the loop simulation
NEDC	New European driving cycle

The associate editor coordinating the review of this manuscript and approving it for publication was Mingjian Cui.

WLTP	Worldwide harmonized light-duty vehicle test procedure
ECM	Electric circuit model
ENN	Equivalent electric network
BEV	Battery-electric vehicle
PI	Proportional integrator
LQI	Linear quadratic integral
SMC	Sliding mode control
MPC	Model predictive control
ARE	Algebraic Riccati equation

I. INTRODUCTION

Electric vehicles (EVs) have obvious advantages with regard to emissions and human health. A larger share of EVs in the future will also have implications on the number of self-driving cars, especially for road transport, relying on cruise control technology. EVs use electrical energy stored in batteries, in which the amount of charge is limited [1]. The entire EV paradigm puts importance on energy efficiency strategy.

One of the energy efficiency strategies of EVs is based on system modeling. This approach models the physical dynamics of the EV system in the form of mathematical equations. Researches on energy efficiency strategies based on the system modeling approach can be classified into two categories.

Firstly, EV models that take into account longitudinal vehicle dynamics. Reference [2] presents a model of the longitudinal dynamics that describes the one-dimensional motion of a point mass, which incorporates the traction force as well as the driving resistance forces. It includes an energy-efficient cruise controller and the energy consumption is modeled implicitly using a kinetic energy formulation. Reference [3] presents an EV model based on the force analysis of the vehicle during a trip. The energy consumption is formulated in a complex function of the vehicle's specifications. Reference [4] proposes an EV model based on the assumption that its energy consumption equals the power required to produce the tractive effort. The energy consumed is estimated by integrating power consumption over time.

Secondly, EV models that take into account the longitudinal vehicle dynamics and electric motor dynamics. Reference [5] proposes EV models with 3-DOF longitudinal vehicle dynamics and an explicit motor model, which only determines the effect of braking torque generated by the in-wheel motors. The energy consumption is estimated by the efficiency between the drive energy and the regenerative energy. Reference [6] presents an EV model with basic longitudinal dynamics, which captures the inertia dynamics of the vehicle and the efficiency of the powertrain components in order to be able to predict energy consumption. The energy consumption is determined from the energy used by the motor. Reference [7] describes an EV model based on vehicle longitudinal dynamics, which includes the overall moment of inertia of the power train, the engine torque, and

the accelerator pedal position. The engine torque is calculated by interpolation of the velocity trajectory and the driver's accelerator pedal position in an energy-optimal manner.

This paper presents a strategy to make the use of battery energy more efficient for EV applications. Our contributions are: (1) formulation of a new approach of EV modeling that includes the battery dynamics into the motor-vehicle model; (2) designing vehicle speed and torque controllers using LQI control and a Kalman filter based on the proposed integrated battery-electric vehicle (IBEV) model; (3) formulation of energy consumption performance indices for EV applications; (4) demonstrating the effectiveness of the proposed approach through a speed-control comparison study involving several test cases, i.e. the two different models in combination with battery used (lithium-ion or lead-acid battery), shaft used (rigid or flexible shaft), and also the combination of LQI controller and observer application; (5) development an EV testbed model. The EV parameter values are adopted from two real EVs and simulations are carried out using a computer and an EV testbed platform based on hardware-in-the-loop (HILS) simulations. Energy performance is evaluated using three vehicle speed profiles, i.e. acceleration from standstill to constant speed, New European Driving Cycle (NEDC), and worldwide harmonized light-duty vehicle test procedure (WLTP).

This paper is organized as follows: the introduction is in Section I, an overview of the EV subsystem is described in Section II. This is followed by an explanation of battery electric-vehicle (BEV) modeling in Section III, and EV control applications in Section IV. The simulation and discussion are presented in Section V. The paper is closed by some concluding remarks in Section VI.

II. OVERVIEW OF EV SUBSYSTEMS

A dynamical model of an EV system generally consists of battery, electric motor, gear train, and longitudinal vehicle dynamics, which together are called the powertrain system [8]. In this section, the dynamics of these subsystems are overviewed; more details can be found in Appendix A and the corresponding references.

In this work, two types of batteries are used, i.e. lithium-ion batteries and lead-acid batteries. The lithium-ion battery circuit can be represented in an electric circuit model (ECM), namely the Thevenin circuit model, which consists of resistors and capacitors [9], [10], as shown in Fig. 1a. Based on Kirchhoff's law, the battery voltage equation can be written as follows:

$$V_b(t) = -R_d i_b(t) - V_{c1}(t) - V_{c2}(t)$$
$$+ 2a_1 SOC_n(t) + (2a_1 + 2a_0) \quad (1)$$

with R_d is the inner resistance, a_1 is the battery voltage when the state of charge (SOC) is 100%, and a_0 is the battery voltage when the SOC is 0%.

A series of lead-acid batteries can be described in an equivalent electric network (EEN), as shown in Fig. 1b.
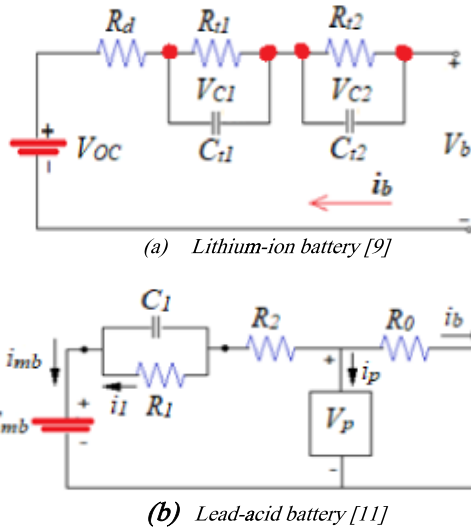
(a) Lithium-ion battery [9]

(b) Lead-acid battery [11]

FIGURE 1. Battery electric circuit.

It consists of extracted charge, electrolyte temperature, and parasitic reaction branches (V_p) [11]. For the discharge process, the parasitic reaction branches can be ignored. Assuming that $i_{mb} = -i_b$, the battery voltage can be written as:

$$V_b(t) = E_{mb0} - R_{00}i_b(t) + (273k_1 + k_1\theta_b(t) - k_2i_1(t)$$
$$+ k_3i_b(t))Q_b(t) \quad (2)$$

where E_{mb0} is open circuit voltage at $SOC = 100\%$, and R_{00} is the value of R_0 at $SOC = 100\%$. Referring to [12] and [13], k_1, k_2, k_3 are suitable constants.

In this work, a BLDC motor is used. The BLDC motor has three stator coils in a Y connected rotor and three permanent magnets. The induction current and the magnetic field harmonics are ignored. The equivalent equation of the motor current can be written as [14], [15]:

$$\frac{di_m(t)}{dt} = -\frac{k_e}{L_m}\omega_m(t) - \frac{R_m}{L_m}i_m(t) + \frac{V_m(t)}{L_m} \quad (3)$$

The developed motor torque can be written as:

$$T_m(t) = k_t i_m(t) \quad (4)$$

with $i_m(t)$ and $V_m(t)$ representing motor current and motor voltage, respectively. $\omega_m(t)$ is motor speed, $L_m = 2(L - M)$ is the equivalent self-inductance, $M = -\frac{L}{2}$ is the mutual inductance of phase, and L is the self-inductance of phase. The equivalent resistance is $R_m = 2R$, where R is the resistance of phase, k_e is the back-emf coefficient, and k_t is the torque coefficient [14], [15].

The gear train subsystem is commonly used to magnify the torque that is transferred from the motor to the wheels. Here, the gear train is described based on two different assumptions, i.e. rigid shaft and flexible shaft. The gear train subsystem circuit with rigid shaft assumption is illustrated in Fig. 2a. It is viewed from the side of shaft 1 (electric motor). The following motor speed equation is obtained [16]:

$$\frac{d\omega_m(t)}{dt} = \frac{1}{J_{eq}}T_m(t) - \frac{b_{eq}}{J_{eq}}\omega_m(t) - \frac{n}{J_{eq}}T_w(t) \quad (5)$$
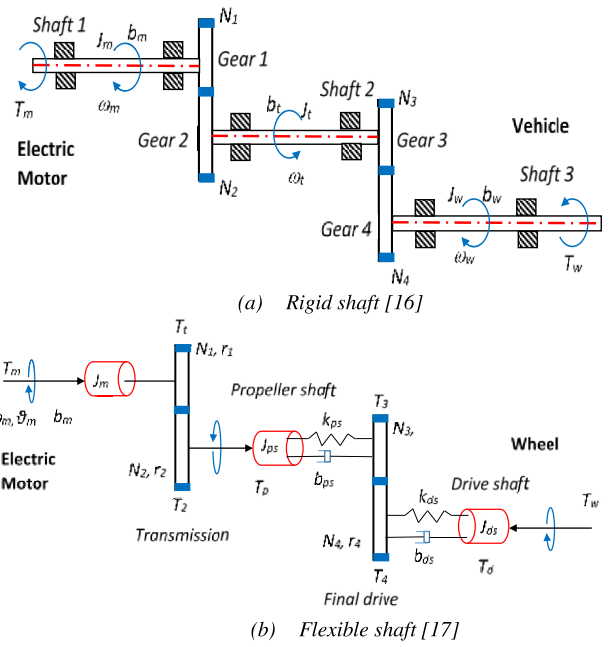

(a) Rigid shaft [16]

(b) Flexible shaft [17]

FIGURE 2. Gear train diagram.

with J_{eq} is the equivalent moment inertia, b_{eq} is the equivalent viscous friction coefficient, and n is the gear ratio.

The flexible shaft of the gear train circuit is illustrated in Fig. 2b. It is viewed from the side of shaft 1 (electric motor). The following motor speed equation is obtained [17]:

$$\frac{d\omega_m(t)}{dt} = \frac{1}{J_{f1}}T_m(t) - \frac{b_{f1}}{J_{f1}}\omega_m(t) + \frac{n_t b_{ps}}{n_g J_{f1}}\omega_d(t)$$
$$- \frac{k_{ps}}{n_g^2 J_{f1}}\theta_m(t) + \frac{n_t k_{ps}}{n_g J_{f1}}\theta_d(t) \quad (6)$$

The final drive's speed is:

$$\frac{d\omega_d(t)}{dt} = -\frac{b_{ds}}{J_{ds}}\omega_d(t) + \frac{b_{ds}}{J_{ds}}\omega_w(t) - \frac{k_{ds}}{J_{ds}}\theta_d(t) + \frac{k_{ds}}{J_{ds}}\theta_w(t) \quad (7)$$

The wheel's speed is:

$$\frac{d\omega_w(t)}{dt} = -\frac{b_{f2}}{J_{f2}}\omega_w(t) + \frac{b_{ds}r_w}{J_{f2}}\omega_d(t) - \frac{k_{ds}r_w}{J_{f2}}\theta_w(t)$$
$$+ \frac{k_{ds}r_w}{J_{f2}}\theta_d(t) + nT_w(t) \quad (8)$$

where k_{ps} and k_{ds} are the propeller position and the final drive position coefficients respectively. J_{f1}, J_{f2}, b_{f1}, and b_{f2}, are suitable constants.

Vehicles mostly make longitudinal movements in carrying out their maneuvers, so that the longitudinal vehicle motion consumes most of the energy compared to the other movements of the vehicle. Therefore, this work only takes longitudinal vehicle motion into account in the modeling.

Our vehicle model is a model of a four-wheel EV, where the mass and tire friction are the same for all four wheels.
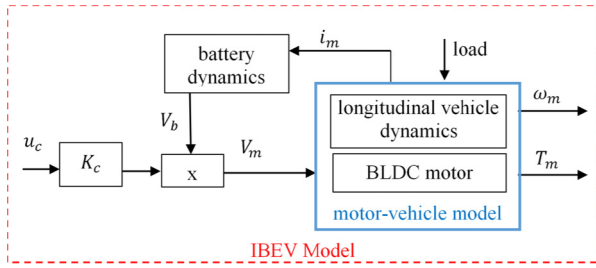
FIGURE 3. BEV models.

The wheel torque is given as follows [8], [18], [19]:

$$
T_w(t) = J_{tot}\frac{d\omega_m}{dt} - n^2 K_d r_w^3 \omega_m^2
$$
$$
- m_v r_w g\left(\sin\theta - C_{Rx}\cos\theta - \frac{k_{tk}}{R}\right) \quad (9)
$$

with J_{tot}, K_d, r_w, m_v, g, C_{Rx}, θ, k_{tk}, and R are suitable constants.

III. BEV MODELING

One of the existing EV models is a model that considers the motor and the longitudinal vehicle dynamics (including drag force), the so-called motor-vehicle model. In this study, this model is further simplified by ignoring the drag force, which will be referred to as the simple model. In addition, we propose a new approach of EV modeling that includes the battery dynamics into a motor-vehicle model and taking into account the drag force. The model is called the Integrated Battery-Electric Vehicle (IBEV) model. Fig. 3 illustrates the BEV modeling scheme, where the motor-vehicle model is described in the blue block while the IBEV model is in the red block.

To study energy consumption through modeling, several EV models are derived with a rigid shaft, with a flexible shaft, without battery, with lithium-ion battery, and with lead-acid battery. These two battery types are chosen because they are widely used batteries. In order to demonstrate the effectiveness of the proposed IBEV model, several speed controllers are also designed. Using the same model, torque control is designed as well. To this aim, we classified the EV models into 6 EV models for speed control mode and 6 EV models for torque control mode, as summarized in Table 1.

Generally, a model is a conceptual representation of a real system in the form of mathematical equations. In the following, the mathematical equations for the simple model with rigid shaft, the simple model with flexible shaft, the IBEV model using a lithium-ion battery and a rigid shaft, the IBEV model using a lithium-ion battery and a flexible shaft, the IBEV model using a lead-acid battery and a rigid shaft, and the IBEV model using a lead-acid battery and a flexible shaft are presented. The details of the suitable constants and state equations can be found in Appendix A and Appendix B, respectively.

TABLE 1. BEV model variations.

Gear train	Battery Type		
	No Battery	Lithium-ion	Lead-acid
Rigid shaft	SMK-1, SMT-1	IMK-1, IMT-1	IMK-2, IMT-2
Flexible shaft	SMK-2, SMT-2	IMK-3, IMT-3	IMK-4, IMT-4
	Simple Model	**IBEV Model**	

Note: SMK: simple model for speed control, SMT: simple model for torque control, IMK: IBEV model for speed control, IMT: IBEV model for torque control.

A. SIMPLE MODEL

The simple models are derived using the motor current and torque equations in (3) and (4), the motor speed equation in (5) for the rigid shaft models or the motor speed equations in (6) to (8) for the flexible shaft models, and the wheel torque equation in (9). The motor speed, $\omega_m(t)$, is used as output for the vehicle speed control, while the motor torque, $T_m(t)$, is used as output for the torque control. The motor voltage $V_m(t)$ is selected as the control input $u_c(t)$ of the EV model. Therefore, the general simple model can be expressed in a state space equation as follows:

$$
\dot{x}_s(t) = A_s x_s(t) + B_s u_c(t) + H_s d_L
$$
$$
y_s(t) = C_s x_s(t) \quad (10)
$$

where C_s is a suitable matrix that is dependent upon the output, either motor speed or motor torque.

1) SIMPLE MODEL WITH RIGID SHAFT

The differential equation of the simple model with rigid shaft refers to the motor current, the motor speed with rigid shaft and the longitudinal vehicle equation.

The state variables are:

$$
x_s = x_a = \begin{bmatrix} x_{a1} & x_{a2} \end{bmatrix}^T \quad (11)
$$

with $x_{a1}(t) = \omega_m(t)$, and $x_{a2}(t) = i_m(t)$.

Based on (10) and (11), the state matrices are:

$$
A_s = A_{s,r} = \begin{bmatrix} a_{a11} & a_{a12} \\ a_{a21} & a_{a22} \end{bmatrix},
$$
$$
B_s = B_{s,r} = \begin{bmatrix} 0 & b_2 \end{bmatrix}^T,
$$
$$
\text{and } H_s = H_{s,r} = \begin{bmatrix} 1 & 0 \end{bmatrix}^T \quad (12)
$$

where

$$
a_{a11} = -\frac{b_{eq}r_w}{nJ_{tot}} \quad a_{a12} = \frac{k_t}{nJ_{tot}} \quad a_{a21} = -\frac{k_e}{L_m}
$$
$$
a_{a22} = -\frac{R_m}{L_m} \quad b_2 = \frac{1}{L_m}.
$$
$$
d_L = -\frac{m_v g r_w}{J_{tot}}\left(\sin\theta + C_{Rx}\cos\theta + \frac{k_{tk}}{R}\right)
$$

b_{eq}, r_w, J_{tot}, k_e, L_m, R_m, L_m, m_v, g, C_{Rx}, k_{tk} and R are suitable constants.

Based on (10) and (11), for simple model with rigid shaft, the output matrices are:

$$C_s = C_{sw,r} = \begin{bmatrix} 1 & 0 \end{bmatrix},$$
$$C_s = C_{sT,r} = \begin{bmatrix} 0 & k_t \end{bmatrix} \qquad (13)$$

$C_{sw,r}$ is the output matrix with the motor speed as output variable. $C_{sT,r}$ is the output matrix with the motor torque as output variable. The simple model with rigid shaft for the motor speed control is called the SMK-1 model, whereas the simple model with rigid shaft for the motor torque control is called the SMT-1 model (see Table 1).

2) SIMPLE MODEL WITH FLEXIBLE SHAFT

The differential equations of the simple model with flexible shaft covers the motor current, the motor speed with the flexible shaft, and the longitudinal vehicle equations.

The state variables are:

$$x_s = \begin{bmatrix} x_a & x_b \end{bmatrix}^T \qquad (14)$$

which $x_a(t)$ as in (11),

$$x_b = \begin{bmatrix} x_{b1} & x_{b2} & x_{b3} & x_{b4} & x_{b5} \end{bmatrix}^T,$$

with $x_{b1}(t) = \omega_d(t)$, $x_{b2}(t) = \omega_w(t)$, $x_{b3}(t) = \theta_m(t)$, $x_{b4}(t) = \theta_d(t)$, and $x_{b5}(t) = \theta_w(t)$.

Based on (10) and (14), for the simple model with flexible shaft, the state matrices are:

$$A_s = A_{bs} = \begin{bmatrix} A_{bs1} & A_{bs2} \\ A_{bs3} & A_{bs4} \end{bmatrix},$$

$$B_s = B_{s,f} = \begin{bmatrix} B_{s,r} \\ 0 \end{bmatrix},$$

$$\text{and } H_s = H_{s,f} = \begin{bmatrix} H_{s,r} \\ 0 \end{bmatrix}$$

where $A_{bs1} = \begin{bmatrix} a_{b11} & a_{b12} \\ a_{b21} & a_{b22} \end{bmatrix}$,

$$A_{bs2} = \begin{bmatrix} a_{b13} & 0 & a_{b15} & a_{b16} & 0 \\ 0 & 0 & 0 & 0 & 0 \end{bmatrix},$$

$$A_{bs3} = \begin{bmatrix} 0 & 0 \\ 0 & a_{b42} \\ 1 & 0 \\ 0 & 0 \\ 0 & 0 \end{bmatrix},$$

$$A_{bs4} = \begin{bmatrix} a_{b33} & a_{b34} & 0 & a_{b36} & a_{b37} \\ a_{b43} & a_{b44} & 0 & a_{b46} & a_{b47} \\ 0 & 0 & 0 & 0 & 0 \\ 1 & 0 & 0 & 0 & 0 \\ 0 & 1 & 0 & 0 & 0 \end{bmatrix}, \quad (15)$$

$B_{s,r}$ and $H_{s,r}$ as in (12), with

$$a_{b11} = -\frac{b_{f1}}{J_{f1}} \quad a_{b12} = \frac{k_t}{J_{f1}} \quad a_{b13} = \frac{n_t b_{ps}}{n_g J_{f1}}$$

$$a_{b15} = -\frac{k_{ps}}{n_g^2 J_{f1}} \quad a_{b16} = \frac{n_t}{n_g J_{f1}} \quad a_{b21} = -\frac{k_e}{L_m}$$

$$a_{b22} = -\frac{R_m}{L_m} \quad a_{b33} = -\frac{b_{ds}}{J_{ds}} \quad a_{b34} = \frac{b_{ds}}{J_{ds}}$$

$$a_{b36} = -\frac{k_{ds}}{J_{ds}} \quad a_{b37} = \frac{k_{ds}}{J_{ds}} \quad a_{b42} = -\frac{k_t}{n J_{f2}}$$

$$a_{b43} = \frac{b_{ds} r_w}{J_{f2}} \quad a_{b44} = -\frac{b_{f2}}{J_{f2}} \quad a_{b46} = \frac{k_{ds} r_w}{J_{f2}}$$

$$a_{b46} = \frac{k_{ds} r_w}{J_{f2}}$$

b_{f1}, b_{f2}, b_{ps}, b_{ds}, J_{f1}, J_{f2}, J_{ds}, k_{ps}, k_{ds}, n_t, and n_g are suitable constants.

Based on (10) and (11), for the simple model with flexible shaft, the output matrices are:

$$C_s = C_{sw,f} = \begin{bmatrix} C_{sw,r} & 0_{1\times5} \end{bmatrix},$$
$$C_s = C_{sT,f} = \begin{bmatrix} C_{sT,r} & 0_{1\times5} \end{bmatrix} \qquad (16)$$

with $C_{sw,r}$ and $C_{sT,r}$ as in (13). $C_{sw,f}$ and $C_{sT,f}$ are the output matrices for motor speed or motor torque as the output, respectively. The simple model with flexible shaft with motor speed control is called the SMK-2 model, whereas the simple model with flexible shaft with motor torque control is called the SMT-2 model (see Table 1).

B. IBEV MODEL

The IBEV models are obtained by incorporating the battery model in Equation (1) for the lithium-ion battery and in Equation (2) for the lead-acid battery together with its corresponding dynamical equations as given in the Appendix into the simple model described in the previous section.

The IBEV models have the nonlinear state space equation in which $F_g(x_g(t))$ includes drag force and $G_g(x_g(t))$ includes the product of battery voltage V_b and motor voltage V_m. Note that V_b depends on the battery type. It is assumed that the battery current is equal to the motor current, i.e.

$$i_b(t) = i_m(t) \qquad (17)$$

The control variable is included in the motor voltage as (see Fig.3),

$$V_m(t) = K_c V_b(t) u_c(t) \qquad (18)$$

The EV models for motor speed or motor torque control have the same state space equations but a different output matrix. The general equation of the IBEV model is given by:

$$\dot{x}_g(t) = F_g(x_g(t)) + G_g(x_g(t)) u_c(t) + H_g d_g$$
$$y_g(t) = C_g x_g(t) \qquad (19)$$

1) IBEV MODEL WITH RIGID SHAFT

The state space equation of the IBEV model with rigid shaft covers the battery variables, the motor current, and the motor speed.

The state variables are:

$$x_{g,r} = \begin{bmatrix} x_a & x_c \end{bmatrix}^T \qquad (20)$$

with $x_a(t)$ as in (11), and x_c are the battery variables. The battery variables for lithium-ion $x_{c,ion}$ can be written as

$$x_{c,ion} = \begin{bmatrix} V_{c1}(t) & V_{c2}(t) & SOC_n(t) \end{bmatrix}^T.$$

Meanwhile, the battery variable for lead-acid $x_{c,acid}$ can be written as

$$x_{c,acid} = \begin{bmatrix} \theta_b(t) & Q_b(t) & i_1(t) \end{bmatrix}^T.$$

Based on (19) and (20), for the IBEV model with rigid shaft, the matrix functions are:

$$F_g = F_{g,r} = \begin{bmatrix} A_{ir,NL} & 0 \\ A_{c1} & A_{c2} \end{bmatrix},$$

$$G_g = G_{g,r} = \begin{bmatrix} B_{i,NL} \\ 0 \end{bmatrix},$$

$$H_g = H_{g,r} = \begin{bmatrix} H_{ir} \\ H_c \end{bmatrix}, \quad \text{and } d_g = \begin{bmatrix} d_L \\ d_\theta \end{bmatrix}. \quad (21)$$

with

$$A_{ir,NL} = \begin{bmatrix} a_{a11} + a_{a11NL} & a_{a12} \\ a_{a21} & a_{a22} \end{bmatrix},$$

where $a_{a11NL} = -K_d r_w^3 x_{a1}^2 / 2J_{tot}$, a_{a11}, a_{a12}, a_{a21}, a_{a22}, d_L as in (12), and K_d is a suitable constant.

A_{c1}, A_{c2}, $B_{i,NL}$, H_{ir}, and H_c matrices are dependent upon the battery type as below.

Lithium-ion battery:

$$A_{c1} = A_{c1,ion} = \begin{bmatrix} 0 & a_{c1,ion} \\ 0 & a_{c2,ion} \\ 0 & a_{c3,ion} \end{bmatrix},$$

$$A_{c2} = A_{c2,ion} = \begin{bmatrix} a_{c4,ion} & 0 & 0 \\ 0 & a_{c5,ion} & 0 \\ 0 & 0 & 0 \end{bmatrix},$$

$$B_{i,NL} = B_{i,NL,ion} = \begin{bmatrix} 0 \\ b_{2NL,ion} \end{bmatrix}, \quad H_{ir} = H_{ir,ion} = \begin{bmatrix} 0 \\ 1 \end{bmatrix},$$

$$H_c = H_{c,ion} = \begin{bmatrix} 0 & 0 & 0 \\ 0 & 0 & 0 \end{bmatrix}^T. \quad (22)$$

with

$$a_{c1,ion} = \frac{1}{C_{t1}} \quad a_{c2,ion} = \frac{1}{C_{t2}} \quad a_{c3,ion} = -\frac{1}{Q_n}$$

$$a_{c4,ion} = -\frac{1}{R_{t1}C_{t1}} \quad a_{c5,ion} = -\frac{1}{R_{t2}C_{t2}}$$

$$b_{2NL\_ion} = b_{c20} + b_{c21}x_{a2} + b_{c22}x_{c1,ion}$$
$$+ b_{c23}x_{c2,ion} + b_{c24}x_{c3,ion}$$

$$b_{c20} = \frac{(2a_0 + 2a_1)K_c}{L_m} \quad b_{c21} = -\frac{R_d K_c}{L_m}$$

$$b_{c22} = -\frac{K_c}{L_m} \quad b_{c23} = -\frac{K_c}{L_m} \quad b_{c24} = \frac{2a_1 K_c}{L_m}$$

C_{t1}, C_{t2}, Q_n, R_{t1}, R_{t2}, a_0, a_1, and R_d, are suitable constants.
Lead-acid battery:

$$A_{c1,acid} = \begin{bmatrix} 0 & a_{c1NL,acid} \\ 0 & a_{c2,acid} \\ 0 & a_{c3NL,acid} \end{bmatrix},$$

$$A_{c2,acid} = \begin{bmatrix} a_{c4,acid} & 0 & 0 \\ 0 & 0 & 0 \\ 0 & a_{c5NL,acid} & 0 \end{bmatrix},$$

$$B_{ir,NL} = B_{ir,NL,acid} = \begin{bmatrix} 0 \\ b_{2NL,acid} \end{bmatrix},$$

$$H_{ir} = H_{ir,acid} = \begin{bmatrix} 0 & 0 \\ 1 & 0 \end{bmatrix},$$

$$H_c = H_{c,acid} = \begin{bmatrix} 0 & 0 & 0 \\ 0 & 1 & 0 \end{bmatrix}^T. \quad (23)$$

with

$$a_{c1NL,acid} = \frac{R_{02}}{C_{\theta b}}x_{a1}(t)^2 \quad a_{c2,acid} = 1$$

$$a_{c3NL,acid} = \frac{x_{b2}}{k_5 x_{c2,acid}} \quad a_{c4,acid} = \frac{1}{C_{\theta b}R_{\theta b}}$$

$$a_{c5NL,acid} = \frac{x_{b5}}{k_5 x_{c2,acid}}$$

$$b_{2NL\_acid} = b_{d20} + b_{d21}x_{a2} + (b_{d22} + b_{d23}x_{c1,acid}$$
$$+ b_{d24}x_{a2} + b_{d25}x_{c3,acid}) x_{c2,acid}.$$

$$b_{d20} = \frac{E_{mb0}K_c}{L_m} \quad b_{d21} = -\frac{R_{00}K_c}{L_m}$$

$$b_{d22} = \frac{273k_1 K_c}{L_m} \quad b_{d23} = \frac{k_1 K_c}{L_m}$$

$$b_{d24} = \frac{k_3 K_c}{L_m} \quad b_{d25} = -\frac{k_2 K_c}{L_m} \quad d_\theta = \frac{\theta_{\alpha b}}{R_{\theta b}C_{\theta b}}$$

R_{02}, $R_{\theta b}$, R_{00}, $C_{\theta b}$, k_1, k_2, k_3, k_5, E_{mb0}, and $\theta_{\alpha b}$ are suitable constants.

Based on (19) and (20), for the IBEV model with rigid shaft, the output matrix is one of the following:

$$C_{gwr,ion} = \begin{bmatrix} C_{sw,r} & 0 \end{bmatrix},$$
$$C_{gTr,ion} = \begin{bmatrix} C_{sT,r} & 0 \end{bmatrix},$$
$$C_{gwr,acid} = \begin{bmatrix} C_{sw,r} & 0 \end{bmatrix},$$
$$C_{gTr,acid} = \begin{bmatrix} C_{sT,r} & 0 \end{bmatrix} \quad (24)$$

with $C_{gwr,ion}$ and $C_{gTr,ion}$ are the output matrices of the models with lithium-ion battery for motor speed and motor torque control, respectively. $C_{gwr,acid}$ and $C_{gTr,acid}$ are the output matrices of the models with lead-acid battery for motor speed and motor torque control, respectively.

The IBEV model with rigid shaft and lithium-ion battery for motor speed control is called the IMK-1 model and for motor torque control is called the IMT-1 model. Meanwhile, the IBEV model with rigid shaft and lead-acid battery for motor speed control is called the IMK-2 and for motor torque control is called the IMT-2 model (see Table 1).

2) IBEV MODEL WITH FLEXIBLE SHAFT

The state space equation of the IBEV model with flexible shaft covers the battery variables, the motor current, the motor speed, and shaft variables.

The state variables are:

$$x_{g,f} = \begin{bmatrix} x_a & x_b & x_c \end{bmatrix}^T \quad (25)$$

with $x_a(t)$ as in (11), x_b as in (14), and x_c as in (20).

Based on (19) and (25), the matrix functions are:

$$F_g = F_{g,f} = \begin{bmatrix} A_{bi,NL} & 0 \\ A_{c1} & A_{c2} \end{bmatrix},$$

$$G_g = G_{g,f} = \begin{bmatrix} B_{i,NL} \\ 0 \end{bmatrix},$$

$$H_g = H_{g,f} = \begin{bmatrix} H_{if} \\ 0 \end{bmatrix}, \quad \text{and } d_g = \begin{bmatrix} d_L \\ d_\theta \end{bmatrix}. \quad (26)$$

with

$$A_{bi,NL} = \begin{bmatrix} A_{bi1} & A_{bi2} \\ A_{bi3} & A_{bi4,NL} \end{bmatrix},$$

A_{bi1}, A_{bi1}, and A_{bi1} are the same as simple model in (15), A_{c1}, A_{c2}, and $B_{i,NL}$ as in (21) and (22).

$$A_{bi4,NL} = \begin{bmatrix} a_{b33} & a_{b34} & 0 & a_{b36} & a_{b37} \\ a_{b43} & a_{b44} + a_{b44,NL} & 0 & a_{b46} & a_{b47} \\ 0 & 0 & 0 & 0 & 0 \\ 1 & 0 & 0 & 0 & 0 \\ 0 & 1 & 0 & 0 & 0 \end{bmatrix},$$

with $a_{b44NL} = -K_d r_w^2 x_{b2}^2 / 2J_{f2}$.

and

$$H_{if} = \begin{bmatrix} 0 & 1 & 0 & 0 & 0 & 0 & 0 \\ 0 & 0 & 0 & 0 & 0 & 0 & 0 \end{bmatrix}^T.$$

Based on (19) and (25), for the IBEV model with flexible shaft, the output matrix is one of the following:

$$C_{gwf,ion} = \begin{bmatrix} C_{sw,f} & 0 \end{bmatrix},$$
$$C_{gwf,ion} = \begin{bmatrix} C_{sT,f} & 0 \end{bmatrix},$$
$$C_{gwf,acid} = \begin{bmatrix} C_{sw,f} & 0 \end{bmatrix},$$
$$C_{gTf,acid} = \begin{bmatrix} C_{sT,f} & 0 \end{bmatrix} \quad (27)$$

with $C_{gwf,ion}$, and $C_{gwf,ion}$ are the output matrices of the models with lithium-ion battery for motor speed and motor torque control, respectively. $C_{gwf,acid}$ and $C_{gTf,acid}$ are the output matrices of the models with lead-acid battery for motor speed and motor torque control, respectively.

The IBEV model with flexible shaft and lithium-ion battery for motor speed control is called IMK-3 model and for the motor torque control is called IMT-3 model. Meanwhile, the IBEV model with flexible shaft and lead-acid battery for motor speed control is called IMK-4 and for the motor torque control is called IMT-4 model (see Table 1).

IV. BEV CONTROL APPLICATIONS

In order to see the energy saving effectiveness, controllers are designed using the models derived in Section III. Reference [20] presents the design of the controllers using PI and LQI control. Both controllers are selected because each one has an integrator to achieve zero steady-state error. The simulation results showed that using an LQI controller consumes less energy than using an PI controller. Reference [21] presents a comparison between the PI controller and a sliding mode controller (SMC). LQI and model predictive control (MPC)

are also compared therein. All of the control designs were built for use with the simple model and the IBEV model.

Based on the application of the controllers in [20] and [21], it is found that the LQI controller is the most beneficial in terms of energy consumption among these controllers, including MPC. Although LQI and MPC are both optimal controllers, the performance index of LQI includes the product of the state variables and inputs, which reflects the energy formulations. Moreover, the computation cost of an LQI controller is much lower than that of an MPC controller. Therefore, the control system used in this work was an LQI controller.

For the case of the IBEV models that are nonlinear, a linearization model was carried out when designing the controllers. Ignoring d_L and d_{θ_b}, the linearized model of (19) can be written as follows:

$$\begin{aligned} \dot{x}_v(t) &= A_v x_v(t) + B_v u_c(t) \\ y_v(t) &= C_v x_v(t) \end{aligned} \quad (28)$$

with A_v, B_v, C_v are suitable matrices and $x_v(t)$, $y_v(t)$ are the state and the output variables of the linearized model, respectively.

Referring to [22], the LQI control is formulated with the following set-point tracking $r(t)$:

$$\dot{x}_i(t) = r(t) - C_v x_v(t) \quad (29)$$

Using (28) and (29), the augmented system can be written as:

$$\dot{x}_z(t) = A_z x_z(t) + B_z u_c(t) + G_z r(t) \quad (30)$$

with

$$A_z = \begin{bmatrix} A_v & 0 \\ -C_v & 0 \end{bmatrix}, \quad B_z = \begin{bmatrix} B_v \\ 0 \end{bmatrix}, \quad G_z = \begin{bmatrix} 0 \\ 1 \end{bmatrix},$$

and $x_z(t) = \begin{bmatrix} x_v(t) & x_i(t) \end{bmatrix}^T$.

The optimal full state feedback control is:

$$u_c(t) = -K_z x_z(t) \quad (31)$$

with $K_z = -R_z^{-1} B_z^T P_z$, which minimizes the following performance index:

$$J = \int_0^\infty (x_z(t)^T Q_z x_z(t) + u_c(t)^T R_z u_c(t)) dt \quad (32)$$

where the weighting matrices $R_z > 0$ and $Q_z \geq 0$. P_z matrix is obtained by solving the ARE as follows:

$$Q_z + A_z^T P_z + P_z A_z - P_z B_z R_z^{-1} B_z^T P_z = 0 \quad (33)$$

Reference [23] designed the LQI controller with a 4th order and a 5th order Luenberger observer using the IBEV model, but both observers were not able to solve the problem of the noise effect on the system and its controller. Therefore, the application of the LQI controller with a Kalman filter is considered in this work. The diagram of the LQI controller with Kalman filter is depicted in Fig. 4.
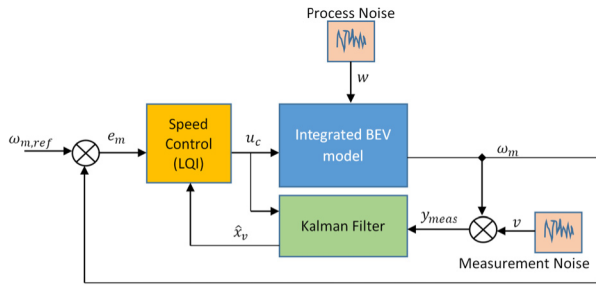
FIGURE 4. The LQI controller with Kalman filter.

Referring to [24], the formulation of the Kalman filter can be stated as follows. The system plant of (30) with disturbances can be written as follows:

$$\dot{x}_v(t) = A_v x_v(t) + B_v u_c(t) + B_w w(t)$$
$$y_b(t) = C_b x_v(t) + v(t) \qquad (34)$$

Process and measurement disturbances $w(t)$ and $v(t)$ are assumed scalars and zero mean Gaussian white noise, with covariances R_{ww} and R_{vv}. Given all measurements $y_v(t)$, the problem of optimal Kalman estimation can be formulated as finding the estimate $\hat{x}_v(t)$, which minimizes the mean square error or error variance:

$$P_e = E\{[x_v(t) - \hat{x}_v(t)][x_v(t) - \hat{x}_v(t)]^T\}. \qquad (35)$$

The form of the optimal estimator is obtained as:

$$\dot{\hat{x}}_v = A_v \hat{x}_v(t) + B_v u_c(t) + L_{kf}(y_v - \hat{y}_v) \qquad (36)$$

The stationary Kalman gain is given by:

$$L_{kf} = P_e C_b^T R_{vv}^{-1} \qquad (37)$$

with P_e is solution of the following ARE:

$$0 = A_v P_e + P_e A_v^T + B_w R_{ww} B_w^T - P_e C_b^T R_{vv}^{-1} C_b P_e \qquad (38)$$

If the estimator (36) is stable and the noise covariances R_{ww} and R_{vv} are constants, then the Kalman gain converges to a constant and P_e satisfies (38).

V. SIMULATION AND DISCUSSION
The simulation is aimed to observe the response characteristics of the system and to study the application schemes that have highest potential to reduce EV energy consumption.

A. ANALYSIS OF ENERGY CONSUMPTION BASED ON THE MODEL
In this subsection we present the numerical parameters of the EV models as listed in Table 1, validate the closed loop system and then analyze the energy consumption. To support the testing of the model and to be able to present the system of a real EV [27], this work used the parameters of the Molina ITB model-3 as in [20], [23], [25], and [26]. Based on type of the battery used, there are two types of Molina ITB model-3. The first vehicle type uses three serially installed 100 Ah /24V lithium-ion batteries (Fig. 5a), and the second vehicle type uses six serially installed 100 Ah/12V lead-acid batteries (Fig. 5b).
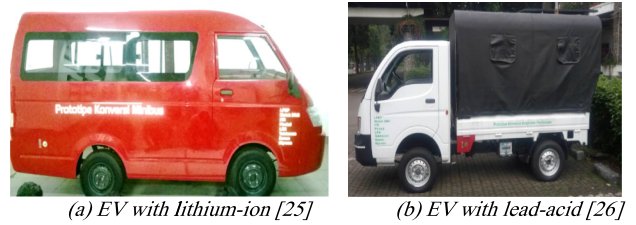

(a) EV with lithium-ion [25]   (b) EV with lead-acid [26]

FIGURE 5. Molina ITB model-3.

1) EV NUMERICAL PARAMETERS
This subsection presents the matrix values of the state-space equation and the output equation of each linear EV model. Six sets of A and B matrices are presented for six linear EV models, i.e. the simple model with rigid shaft, the simple model with flexible shaft, the linearized IBEV model with lithium-ion battery and rigid shaft, the linearized IBEV model with lead-acid battery and rigid shaft, the linearized IBEV model with lithium-ion battery and flexible shaft, and the linearized IBEV model with lead-acid battery and flexible shaft. For controller design preparation, the C matrix for the output equation of each linear EV model is also presented. Notice that each linear EV model has two C matrices. They are for vehicle speed control and torque control.

a: SIMPLE MODEL WITH RIGID SHAFT
Based on (12) and (13), the following matrices are given:

$$A_{s,r} = \begin{bmatrix} -19.82 & 8.34 \\ -3.76 & -3.65 \end{bmatrix}, \quad B_{s,r} = \begin{bmatrix} 0 \\ 905.9 \end{bmatrix}$$

SMK-1: $C_{sr,w} = \begin{bmatrix} 1 & 0 \end{bmatrix}$
SMT-1: $C_{sr,T} = \begin{bmatrix} 0 & 0.078 \end{bmatrix}$

b: SIMPLE MODEL WITH FLEXIBLE SHAFT
Based on (15) and (16), the following matrices are given:

$$A_{bs1} = \begin{bmatrix} -159.5 & 2182 \\ -3.76 & -3.65 \end{bmatrix},$$

$$A_{bs2} = \begin{bmatrix} 8.07 & 0 & -8.58 \times 10^{-5} & 2.02 \times 10^4 & 0 \\ 0 & 0 & 0 & 0 & 0 \end{bmatrix},$$

$$A_{bs3} = \begin{bmatrix} 0 & 0 \\ 0 & -4.64 \times 10^{-2} \\ 1 & 0 \\ 0 & 0 \\ 0 & 0 \end{bmatrix},$$

$$A_{bs4} = \begin{bmatrix} -5.98 \times 10^{-3} & -5.98 \times 10^{-3} & 0 & -1.49 \times 10^{-4} & -1.49 \times 10^{-4} \\ 3.40 \times 10^{-5} & -0.98 & 0 & 8.50 \times 10^{-5} & -8.50 \times 10^{-5} \\ 0 & 0 & 0 & 0 & 0 \\ 1 & 0 & 0 & 0 & 0 \\ 0 & 1 & 0 & 0 & 0 \end{bmatrix}$$

$$B_{s,f} = \begin{bmatrix} 0 & 294.1 & 0 & 0 & 0 & 0 & 0 \end{bmatrix}^T,$$

SMK-2: $C_{sf,w} = \begin{bmatrix} 1 & 0 & 0 & 0 & 0 & 0 & 0 \end{bmatrix}$,
SMT-2: $C_{sf,T} = \begin{bmatrix} 0 & 0.078 & 0 & 0 & 0 & 0 & 0 \end{bmatrix}$,

c: LINEARIZED IBEV MODEL WITH RIGID SHAFT & LITHIUM-ION BATTERY

For an input signal of 24 volt, the operating point is obtained at: $\begin{bmatrix} \omega_m & i_m & V_{c1} & V_{c2} & SOC_n \end{bmatrix}$,

in $\begin{bmatrix} 1720 & 148 & 0.15 & 0.15 & 99.96 \end{bmatrix}$, and based on (21), (22) and (24) the linearized matrices are as follows:

$$A_{ir,NL,ion} = \begin{bmatrix} -0.401 & 1604 \\ -0.019 & -3.941 \end{bmatrix},$$

$$A_{c1,ion} = \begin{bmatrix} 0 & 0 & 0 \\ -0.25 & -0.25 & -0.023 \end{bmatrix}$$

$$A_{c2,ion} = \begin{bmatrix} 0 & 294.1 \\ 0 & 294.1 \\ 0 & 294.1 \end{bmatrix},$$

$$A_{c3,ion} = \begin{bmatrix} -0.291 & 0 & 0 \\ 0 & -0.291 & 0 \\ 0 & 0 & 0 \end{bmatrix}$$

$$B_{vr,ion} = \begin{bmatrix} 0 & 0.802 & 0 & 0 & 0 \end{bmatrix}^T$$

IMK-1: $C_{vr,ion\_w} = \begin{bmatrix} 1.52 & 0 & 0 & 0 & 0 \end{bmatrix}$,

IMT-1: $C_{vr,ion\_T} = \begin{bmatrix} 0 & 294.1 & 0 & 0 & 0 \end{bmatrix}$,

d: LINEARIZED IBEV MODEL WITH RIGID SHAFT & LEAD-ACID BATTERY

For an input signal of 24 volt, the operating point is obtained at: $\begin{bmatrix} \omega_m & i_m & \theta_b & Q_b & i_1 \end{bmatrix}$,

in $\begin{bmatrix} 1720 & 148 & 4824 & 741 & 4 \end{bmatrix}$, and based on (21), (23) and (24) the linearized matrices are as follows:

$$A_{ir,NL,acid} = \begin{bmatrix} -0.39 & 1604 \\ -0.019 & -10.71 \end{bmatrix},$$

$$A_{c1,acid} = \begin{bmatrix} 0 & 0 & 0 \\ 8.27x10^{-4} & -0.016 & 0.0012 \end{bmatrix}$$

$$A_{c2,acid} = \begin{bmatrix} 0 & 19.61 \\ 0 & 294.1 \\ 0 & -0.29 \end{bmatrix},$$

$$A_{c3,acid} = \begin{bmatrix} -0.33 & -4.73x10^{-4} & 0 \\ 0 & 0 & 0 \\ 6.67x10^{-5} & -3.36x10^{-4} & -9.81x10^{-4} \end{bmatrix}$$

$$B_{vr,acid} = \begin{bmatrix} 0 & 0.817 & 0 & 0 & 0 \end{bmatrix}^T$$

IMK-2: $C_{vr,acid\_w} = \begin{bmatrix} 1.52 & 0 & 0 & 0 & 0 \end{bmatrix}$,

IMT-2: $C_{vr,acid\_T} = \begin{bmatrix} 0 & 294.1 & 0 & 0 & 0 \end{bmatrix}$.

e: LINEARIZED IBEV MODEL WITH FLEXIBLE SHAFT & LITHIUM-ION BATTERY

For an input signal of 24 volt, the operating point is obtained at $\begin{bmatrix} \omega_m & i_m & \omega_d & \omega_w & \theta_m & \theta_d & \theta_w & V_{c1} & V_{c2} & SOC_n \end{bmatrix}$, in [1751 148 110 110 1740 990 993 0.12 0.12 99.93], and based on (26) and (27) the linearized matrices are as follows:

$$A_{bi1} = \begin{bmatrix} -159.5 & 31.82 \\ -258.1 & -3.94 \end{bmatrix},$$

$$A_{bi2} = \begin{bmatrix} 30.18 & 0 & -2.99x10^{-5} & 0 & 0 \\ 0 & 0 & 0 & 0 & 0 \end{bmatrix}$$

$$A_{bi3} = \begin{bmatrix} 0 & 0 \\ 0 & 1604 \\ 2016 & 0 \\ 0 & 0 \\ 0 & 0 \end{bmatrix},$$

$$A_{bi4} = \begin{bmatrix} -30.18 & 0.17 & 0 & -1x10^{-5} & 0 \\ 30.18 & -0.98 & 0 & 0 & -1x10^{-5} \\ 0 & 0 & 0 & 0 & 0 \\ 7544 & 0 & 0 & 0 & 0 \\ 0 & 0.43 & 0 & 0 & 0 \end{bmatrix},$$

$$B_{vf,ion} = \begin{bmatrix} 0 & 1 & 0 & 0 & 0 & 0 & 0 \end{bmatrix}^T,$$

IMK-3: $C_{vf,ion\_w} = \begin{bmatrix} 2016 & 0 & 0 & 0 & 0 & 0 & 0 \end{bmatrix}$,

IMT-3: $C_{vf,ion\_T} = \begin{bmatrix} 0 & 294.1 & 0 & 0 & 0 & 0 & 0 \end{bmatrix}$,

f: LINEARIZED IBEV MODEL WITH FLEXIBLE SHAFT & LEAD-ACID BATTERY

For an input signal of 24 volt, the operating point is obtained at $\begin{bmatrix} \omega_m & i_m & \omega_d & \omega_w & \theta_m & \theta_d & \theta_w & \theta_b & Q_b & i_1 \end{bmatrix}$, in [1751 148 110 110 1740 990 993 4824 741 4], and based on (26), and (27) the linearized matrices are as follows:

$$A_{bi1NL} = \begin{bmatrix} -159.5 & 31.82 \\ -258.1 & -10.71 \end{bmatrix},$$

$$A_{bi2} = \begin{bmatrix} 30.18 & 0 & -2.99x10^{-5} & 0 & 0 \\ 0 & 0 & 0 & 0 & 0 \end{bmatrix}$$

$$A_{bi3} = \begin{bmatrix} 0 & 0 \\ 0 & 1604 \\ 2016 & 0 \\ 0 & 0 \\ 0 & 0 \end{bmatrix},$$

$$A_{bi4} = \begin{bmatrix} -30.18 & 0.17 & 0 & -1x10^{-5} & 0 \\ 30.18 & -0.98 & 0 & 0 & -1x10^{-5} \\ 0 & 0 & 0 & 0 & 0 \\ 7544 & 0 & 0 & 0 & 0 \\ 0 & 0.43 & 0 & 0 & 0 \end{bmatrix},$$

$$B_{v,acid} = \begin{bmatrix} 0 & 0.917 & 0 & 0 & 0 & 0 & 0 \end{bmatrix}^T,$$

IMK-4: $C_{vf,acid\_w} = \begin{bmatrix} 2016 & 0 & 0 & 0 & 0 & 0 & 0 \end{bmatrix}$,

IMT-4: $C_{vf,acid\_T} = \begin{bmatrix} 0 & 294.1 & 0 & 0 & 0 & 0 & 0 \end{bmatrix}$,

2) CONTROLLER IMPLEMENTATION

The LQI controllers are designed using the models obtained in the previous section. Each controller is then applied to the nonlinear IBEV model. Due to limited space, only speed control is presented. However, torque control can be done by the same method. This section compares six speed controller test cases executed by means of computer simulations and an EV testbed platform based on hardware-in-the-loop simulations (HILS) [21], as shown in Fig. 6.

In order to make a fair comparison between the test cases, each controller is designed in such a way that they provide the similar vehicle speed time response, as can be seen in Fig. 7a.
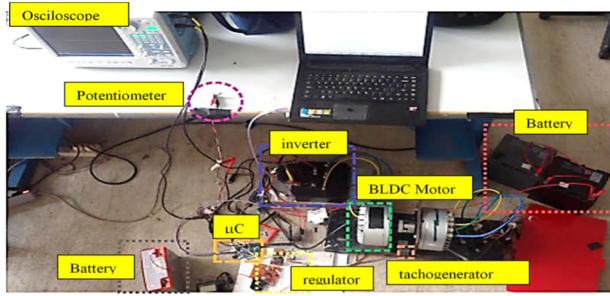
FIGURE 6. EV testbed platform [21].

The similar time response is obtained by selecting appropriate weighting matrices Q_z and R_z. Based on (26) to (27), the weighting matrix values of all speed controllers (SMK-1, SMK-2, IMK-1, IMK-2, IMK-3, IMK-4) are:

SMK-1: Simple model with rigid shaft
For weighting matrix $R_z = 1000$, and

$$Q_z = \begin{bmatrix} 1 & 0 & 0 \\ 0 & 1 & 0 \\ 0 & 0 & 1 \end{bmatrix},$$

is given by gain at

$$K_z = \begin{bmatrix} 0.008 & 0.022 & -0.032 \end{bmatrix}.$$

SMK-2: Simple model with flexible shaft
For weighting matrix $R_z = 1000$, and

$$Q_z = \begin{bmatrix} I_{7\times7} & 0_{7\times1} \\ 0_{1\times7} & 100 \end{bmatrix},$$

is given by gain at

$$K_z = \begin{bmatrix} 0.68 & 0.16 & 0.33 & 0.15 & 0.03 & 0.04 & 0.03 & -490 \end{bmatrix}.$$

IMK-1: IBEV model with rigid shaft & lithium ion
For weighting matrix $R_z = 0.1$, and
$Q_z = [I_{6\times6}]$, is given by gain at
$K_z = \begin{bmatrix} 3.30 & 18.86 & 0.11 & 0.11 & 3.16 & -0.03 \end{bmatrix}$.

IMK-3: IBEV model with flexible shaft & lithium ion
For weighting matrix $R_z = 10$, and

$$Q_z = \begin{bmatrix} I_{10\times10} & 0_{10\times1} \\ 0_{1\times10} & 10 \end{bmatrix},$$

is given by gain at

$$K_z = \begin{bmatrix} K_{z1} & K_{z2} \end{bmatrix}$$
$$K_{z1} = \begin{bmatrix} 0.06 & 0.02 & 0.02 & 0.003 & 0.003 & 0.003 \end{bmatrix}$$
$$K_{z2} = \begin{bmatrix} 1.12 & 0.09 & 0.009 & 0.11 & -0.69 \end{bmatrix}$$

IMK-2: IBEV model with rigid shaft & lead acid
For weighting matrix $R_z = 10$, and

$$Q_z = \begin{bmatrix} 0.1_{5\times5} & 0_{5\times1} \\ 0_{1\times5} & 10 \end{bmatrix},$$

is given by gain at

$$K_z = \begin{bmatrix} 0.97 & 4.85 & 0.001 & 0.005 & 0.001 & -0.98 \end{bmatrix}.$$

IMK-4: IBEV model with flexible shaft & lead acid
For weighting matrix $R_z = 100$, and

$$Q_z = \begin{bmatrix} I_{10\times10} & 0_{10\times1} \\ 0_{1\times10} & 10 \end{bmatrix},$$

is given by gain at

$$K_z = \begin{bmatrix} K_{z1} & K_{z2} \end{bmatrix}$$
$$K_{z1} = \begin{bmatrix} 0.68 & 0.012 & 0.002 & 0.02 & 0.03 & 0.002 \end{bmatrix}$$
$$K_{z2} = \begin{bmatrix} 0.16 & 0.002 & 0.05 & 0.03 & -1.98 \end{bmatrix}.$$

The scenario is to accelerate the vehicle on a flat surface driving profile from standstill condition to constant speed at 60 km/hour for 15 seconds, as shown in Fig. 7a. The vehicle speed shows similar transient response for all models. The motor speed response reaches about 3000 rpm, as shown in Fig. 7b. The motor speed has a settling time of about 4 seconds for SMK-1 and IMK-1, 3 seconds for IMK-2, and 2 seconds for SMK-2, IMK-3 and IMK-4.

The motor current responses are shown in Fig.7d. The models with flexible shaft, i.e. SMK-2, IMK-3 and IMK-4 have better responses in reaching steady state than the models with rigid shaft, i.e. SMK-1, IMK-1, and IMK-2. The models with rigid shaft have about 2 seconds of overshoot. This means that the models with a flexible shaft can reduce overshoot in the motor current response.

The response of the batteries can be seen in Figs. 7e and 7f. In Fig. 7e, it can be seen that the battery's *SOC* decreases slower for the IMK-1 and IMK-3 models than for the other models. The battery *SOC* of IMK-2 and IMK-4 models decreases about 10% faster than that of the IMK-1 and IMK-3 models. Fig. 7f shows that the battery voltage has the same time response for IMK-1 and the IMK-3. The same is the case for IMK-2 and the IMK-4. The above battery responses illustrate the energy consumption described below.

3) ANALYSIS OF ENERGY CONSUMPTION
The energy consumption is calculated using a computer simulation. Besides the driving profile of acceleration on a flat surface described in the previous subsection, 2 other driving profiles are also simulated, i.e. NEDC and WLTP. For comparison, each controller is operated under the same environmental conditions and driving profile.
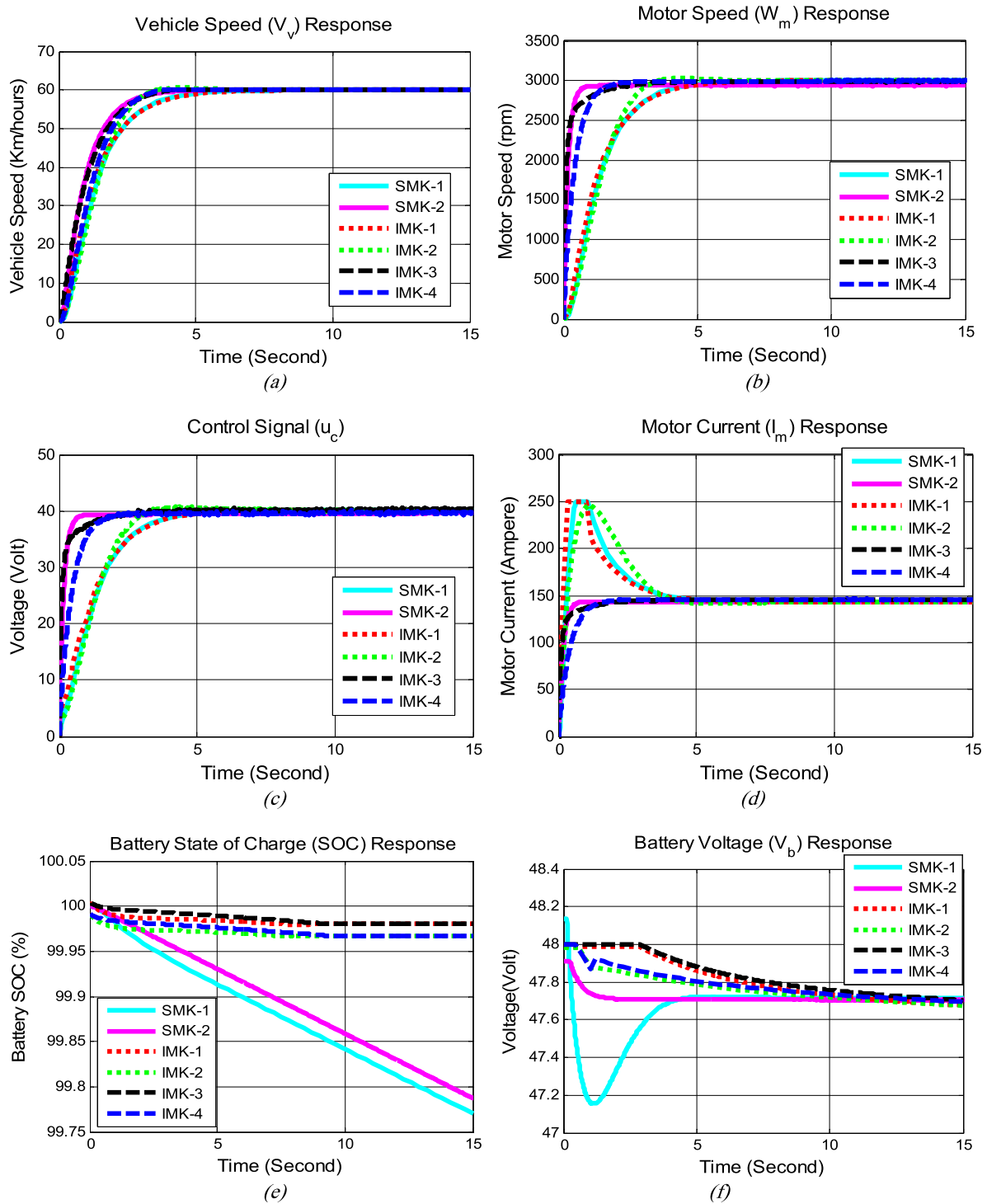
The energy consumption is calculated using the following performance indices.
- Control energy:

$$E_1(t) = \int_0^\infty V_m(t)^2 dt \text{ or}$$
$$J_1 = \int_0^\infty u_c^2 dt \tag{39}$$

- Mechanical energy:

$$E_2(t) = \int_0^\infty T_m(t)\omega_m(t)dt \text{ or}$$
$$J_2 = \int_0^\infty x_{a2}x_{a1}dt \tag{40}$$

FIGURE 7. Comparison of EV model responses using LQI controllers. SMK1: Simple model (rigid shaft), SMK2: Simple model (flexible shaft), IMK1: Integrated model (rigid shaft–lithium), IMK2: Integrated model (rigid shaft–lead acid), IMK3: Integrated model (flexible shaft–lithium), IMK4: Integrated model (flexible shaft–lead acid).

- Electrical energy:

$$E_3(t) = \int_0^\infty V_m(t)i_m(t)dt \text{ or}$$

$$J_3 = \int_0^\infty u_c x_{a2} dt. \tag{41}$$

- Battery energy $E_4(t) = \int_0^\infty V_b(t)i_m(t)dt$ or

Lithium-ion:

$$J_{4,ion} = \int_0^\infty (SOC_n - V_{c1} - V_{c2} - x_{a2}) x_{a2} dt \tag{42a}$$
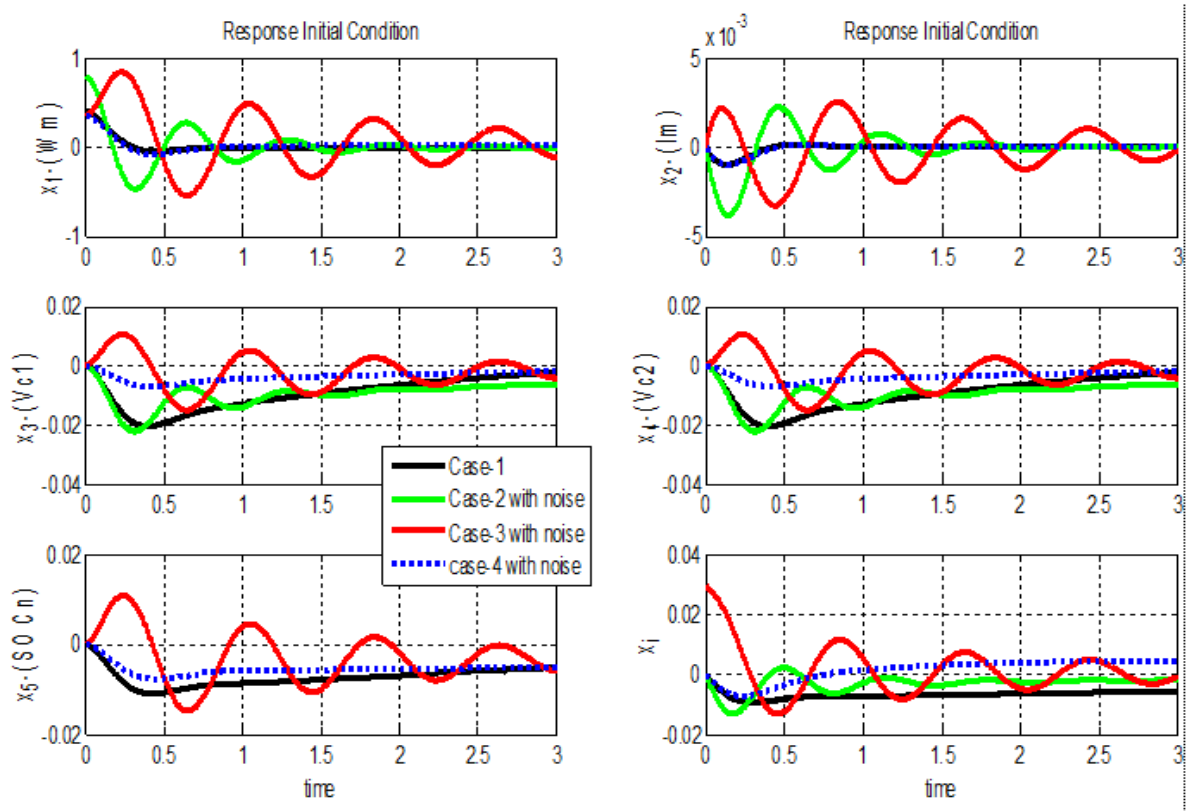
FIGURE 8. EV LQI with observer design response Case-1: LQI controller, Case-2: LQI controller with observer order 4, Case-3: LQI controller with observer order 5, Case-4: LQI controller with Kalman filter.

Lead-acid:

$$J_{4,acid} = \int_0^\infty \left(Q_b + Q_b\theta_b - Q_bi_1 + Q_bx_{a2} - x_{a2} \right) x_{a2}dt$$

$$(42b)$$

Table 2 lists the values of the energy performance indices for the three driving profiles. By observing the individual values and comparing each value to the others, we can see the following three relationships. Firstly, the models using a flexible shaft (SMK2, IMK-3, IMK-4) consumes less energy than the corresponding models that use a rigid shaft (SMK-1, IMK-1, IMK-2). For SMK-2 (flexile shaft) energy consumption is lower than for SMK-1 (rigid shaft) by about 9.2% (J_1), 9.6% (J_2), 9.5% (J_3) and 9.8% (J_4). For the flexible shaft models (IMK-3, IMK-4) it is lower than for the rigid shaft models (IMK-1, IMK2) by about 8.13% (J_1), 8.22% (J_2), 8.13% (J_3), and 8.11% (J_4).

However, further evaluation reveals that the difference in energy consumption between the models using a flexible shaft and a rigid shaft is less than 10%. Thus, the model using a rigid shaft can still represent the EV dynamics, whose mathematical equation is simpler than that of the corresponding model using a flexible shaft.

Secondly, the model using a lithium-ion battery (IMK-1, IMK-3) is more energy efficient than the corresponding model that uses a lead-acid battery (IMK-2, IMK-4).

Referring to Fig. 7d, it can be seen that the motor current of (IMK-2, IMK-4) has a better transient response than (IMK-1, IMK-3), while (IMK-1, IMK-3) has an overshoot that is still below the maximum limit of the motor current. Let us associate these results with Fig. 7e for the driving profile of acceleration on a flat surface. Notice that the *SOC* of the lithium-ion battery decreases slower than that of the lead-acid battery for both models that use rigid and flexible shafts.

Table 2 shows that (IMK-1, IMK-3) consumes less energy than (IMK-2, IMK-4) by 21.34% (J_1), 22.63% (J_2), 23.18% (J_3), and 21.88% (J_4). Thus, it can be concluded that the motor/vehicle speed control using the IBEV models with lithium-ion battery (IMK-1, IMK-3) consumes less energy than the IBEV models with lead-acid battery (IMK-2, IMK-4).

Thirdly, the IBEV models with lithium-ion battery (IMK-1, IMK-3) and the IBEV models with lead-acid battery (IMK-2, IMK-4) consumes less energy than the corresponding simple models (SMK-1, SMK-2).

A further analysis reveals that IMK-1 consumes less energy than SMK-1 and that IMK-2 consumes less energy than SMK-2 by 46.44% (J_1), 48% (J_2), 47.33% (J_3), and 48.67% (J_4).

In general, the IBEV model consumes less energy than the simple model. The IBEV model with lithium-ion battery is preferable over the IBEV model with lead-acid battery.

TABLE 2. Energy consumption.

Model	Energy consumption (Wh)			
	J_1	J_2	J_3	J_4
Flat surface profile (15 seconds)				
SMK-1	1.674×10^3	2.512×10^3	2.765×10^3	2.955×10^3
SMK-2	1.540×10^3	2.415×10^3	2.626×10^3	2.895×10^3
IMK-1	0.823×10^3	1.196×10^3	1.335×10^3	1.393×10^3
IMK-2	0.896×10^3	1.303×10^3	1.456×10^3	1.516×10^3
IMK-3	0.705×10^3	0.925×10^3	1.025×10^3	1.088×10^3
IMK-4	0.925×10^3	1.008×10^3	1.119×10^3	1.184×10^3
NEDC profile (1200 seconds)				
SMK-1	2.938×10^3	4.025×10^3	4.237×10^3	4.323×10^3
SMK-2	2.703×10^3	3.864×10^3	4.025×10^3	4.236×10^3
IMK-1	1.445×10^3	1.916×10^3	2.046×10^3	2.039×10^3
IMK-2	1.573×10^3	2.088×10^3	2.231×10^3	2.218×10^3
IMK-3	1.137×10^3	1.482×10^3	1.571×10^3	1.592×10^3
IMK-4	1.237×10^3	1.615×10^3	1.714×10^3	1.733×10^3
WLTP profile (1800 seconds)				
SMK-1	5.318×10^3	7.286×10^3	7.669×10^3	7.826×10^3
SMK-2	4.892×10^3	6.994×10^3	7.285×10^3	7.669×10^3
IMK-1	2.616×10^3	3.469×10^3	3.703×10^3	3.691×10^3
IMK-2	2.848×10^3	3.779×10^3	4.039×10^3	4.017×10^3
IMK-3	2.058×10^3	2.684×10^3	2.845×10^3	2.883×10^3
IMK-4	2.240×10^3	2.924×10^3	3.102×10^3	3.138×10^3

In terms of model simplicity, the IBEV model with rigid shaft is preferable over the corresponding model with flexible shaft.

B. ANALYSIS OF NOISE EFFECT

In this subsection, LQI controllers with observers are presented for the IBEV model with lithium-ion battery and rigid shaft (the IMK-1 model). The LQI controller with Kalman filter is designed and its performance is compared to LQI controllers with Luenberger observers of order 4 and order 5 that have been designed previously [23].

The Kalman Filter is designed by giving the measurement noise covariance $R_{vv} = 0.2$ and the process noise covariance $R_{ww} = 0.2$. Based on (37) and (38) the matrix weight $Q_e = 0.02$ obtained by the Kalman gain is $L_{kf} = \begin{bmatrix} 27.25 & 0.36 & 5.01 & 5.01 & 4.99 \end{bmatrix}^T$, and the eigenvalues of the estimator are $-4.29+6.56i$, $-4.29-6.56i$, -1.35, -0.05, -0.290, -0.291, $-25.50+23.64i$, $-25.50-23.64i$, -0.042, -0.291, and -0.291.

The LQI controller with Kalman filter is compared with the LQI controller without observer and the LQI controllers with Luenberger observers previously designed in [23]. All the controllers are simulated with white noise added. We will call the case of the LQI controller *case-1*, the LQI controller with 4th order Luenberger observer will be called *case-2*, the LQI controller with 5th order Luenberger observer will be called *case-3*, and the LQI controller with Kalman filter will be called *case-4*.

In order to evaluate the noise rejection capability, the initial value responses of the 6 state variables under the white noise influence are plotted in Fig. 8. Case-3 seems to have a fluctuating response due to the noise while case-2 and case-4 do not show any noise effect. The motor speed (state
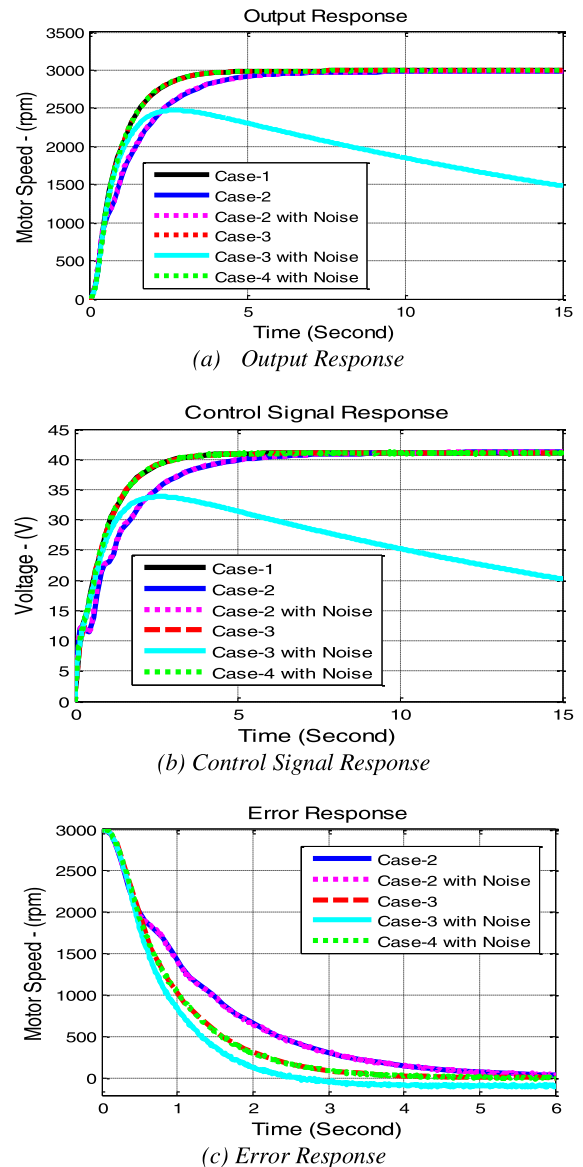
(a) Output Response

(b) Control Signal Response

(c) Error Response

FIGURE 9. LQI and its designed observer response.

variable 1) and the motor electric current (state variable 2) of the LQI controller with Kalman filter demonstrate the similar initial responses as those of the standard LQI controller without observer. As expected, these results show that the use of a Kalman filter can enhance the noise rejection capability of the LQI controllers.

Vehicle speed performance and energy consumption are evaluated by conducting simulations using the above 4 cases for the driving profile of acceleration on a flat surface. The output responses in Fig. 9a and the control signal responses in Fig. 9b have the similar responses with an approximate settling time of about 2 seconds for case-1 (black line), case-3 (red line) and case-4 (green line). Case-2 (blue line) and case-2 with noise (magenta line) are a bit slow to reach steady state, with a settling time of around 5 seconds. Case-3 with noise (cyan line) cannot reach steady state and instead moves away

TABLE 3. Energy consumption for LQI with observer.

Case	Energy Consumption (Wh)	
	J2	J3
1 (LQI without observer)	2.205×10^3	2.808×10^3
2 (LQI with 4th order observer)	1.935×10^3	1.944×10^3
2 (LQI with 4th order observer and noise)	2.331×10^3	2.581×10^3
4 (LQI with Kalman Filter and noise)	1.732×10^3	1.781×10^3

from the given set point. Fig. 9c shows the time responses of the motor speed estimation errors of each observer with and without noise influence. From these results the LQI controller with 5th order Luenberger observer (case-3) is excluded from further analysis since it shows poor noise rejection capability. This means that case-4 can reduce noise and has a good system response.

The energy consumptions of case-1 (without observer) and case-2 and case-4 (with observer) are calculated using mechanical energy and electrical energy performance indices. The results are listed in Table 3. Case-4 with noise and case-1 have the similiar responses, as can be seen in Fig. 9a. Case-4 consumes less energy by 27.31% (J2), and 57.66% (J3) compared to case-1. Thus, it can be said that case-4 has an accurate response and is more economical than the controllers with other observers.

VI. CONCLUDING REMARKS

A new strategy for reducing the energy consumption of the battery in an electric vehicle is presented in this paper. The strategy is to use an EV model, called IBEV model, in designing a controller. The IBEV model is a model that integrates the battery dynamics into the motor-vehicle dynamics. In order to increase the usefulness of the model, a controller is designed using a standard LQI control for either speed or torque control based on linear or linearized models. The designed controllers are tested on a nonlinear IBEV model.

From the model testing, it is found that the IBEV model for speed control consumes less energy than using the simple model. In addition, it is found that the EV model with a flexible shaft in the gear train system has a good characteristic response and consumes 10% less energy compared to the EV model with a rigid shaft. In terms of controller complexity, the EV model with a rigid shaft can be chosen as the basis for the design of a controller. In terms of the battery type used, it is found that the IBEV model with lithium-ion batteries consumes less energy than with lead-acid batteries. The LQI with Kalman filter reduces the noise effect, has a good system response and is more economical than the controllers with other observers.

APPENDIX A
EV SUBSYSTEMS

An EV system generally consists of battery, electric motor, gear train, and longitudinal vehicle dynamics subsystems.

An overview of these subsystems is described in the body of this article. The details are as follows:

Lithium-ion Battery

The dynamical equations of voltage and the *SOC* of the lithium-ion batteries are:

$$\frac{dV_{c1}(t)}{dt} = -\frac{1}{R_{t1}C_{t1}}V_{c1}(t) + \frac{1}{C_{t1}}i_b(t)$$

$$\frac{dV_{c2}(t)}{dt} = -\frac{1}{R_{t2}C_{t2}}V_{c2}(t) + \frac{1}{C_{t2}}i_b(t)$$

$$\frac{dSOC_n(t)}{dt} = -\frac{1}{Q_n}i_b(t)$$

where R_{t1} is 1st terminal resistor, R_{t2} is 2nd terminal resistor, C_{t1} is 1st terminal capacitor, C_{t2} is 2nd terminal capacitor, and Q_n is the capacity of lithium-ion [9], [10].

Lead-acid Battery

The dynamical equations of electrolyte temperature $\theta_b(t)$, extracted charge $Q_b(t)$, *SOC* and current branch $i_1(t)$ are:

$$\frac{d\theta_b(t)}{dt} = \frac{R_{02}}{C_{\theta b}}i_b(t)^2 - \frac{1}{R_{\theta b}C_{\theta b}}\theta_b(t) + \frac{\theta_{\alpha b}}{R_{\theta b}C_{\theta b}}$$

$$\frac{dQ_b(t)}{dt} = i_b(t)$$

$$SOC = 1 - \frac{Q_b}{Q_{0b}}$$

$$\frac{di_1(t)}{dt} = \frac{1}{k_2 C_1 Q_b(t)}(i_b(t) + i_1(t))$$

with $k_1 = \frac{K_E}{Q_{0b}}$, $k_2 = R_{10}\ln(-\frac{1}{Q_{nb}})$, and

$$k_3 = \frac{R_{00}A_0 \exp\left[A_{21}\left(-\frac{1}{Q_{0b}}\right)\right]}{1 + \exp\left(\frac{A_{22}I_{mb}}{I^*}\right)}$$

where R_{02} is the 2nd inner branch resistance, $R_{\theta b}$ is the thermal battery resistance, $C_{\theta b}$ is the thermal battery capacitance, $\theta_{\alpha b}$ is the ambient temperature, C_1 is the 1st main branch capacitance, K_E is a constant, Q_{0b} is the capacity in the electrolyte temperature at full charge, R_{10} is a constant of R_1, Q_{nb} is the capacity in the electrolyte temperature at time t, R_{00} is the value of R_0 at $SOC = 1$, A_0, A_{21}, A_{22} are constants, I_{mb} is the main branch current, I* is the nominal battery current, R_1 is the main branch resistance 1, and R_0 is the inner resistance [11]–[13].

Rigid Shaft

The equivalent moment inertia J_{eq} and the equivalent viscous friction coefficient b_{eq} are given by:

$$J_{eq} = J_m + \frac{J_t}{n_g^2} + \frac{J_w}{n_g^2 n_t^2}$$

$$b_{eq} = b_m + \frac{b_t}{n_g^2} + \frac{b_w}{n_g^2 n_t^2}$$

where J_m, J_t and J_w are the inertia of the motor, the transmission and the wheels, respectively. b_m, b_t and b_w are the viscous friction of the motor, the transmission and the wheels, respectively. n_t and n_g are the gear ratio of the transmission and the gearbox, respectively [16].

Flexible Shaft

The equivalent inertias J_{f1} and J_{f2}, and the equivalent viscous friction coefficients b_{f1} and b_{f2} are given by:

$$J_{f1} = \left(J_m + \frac{J_{ps}}{n_g^2}\right)$$

$$J_{f2} = r_w\left(m_v r_w + J_w\right)$$

$$b_{f1} = \left(b_m + \frac{b_{ps}}{n_g^2}\right)$$

$$b_{f2} = r_w\left(b_w + b_{ds}\right)$$

with J_{ps}, J_{ds} and J_w are the inertia of the propeller, the final drive, and the wheels, respectively. b_{ps}, b_{ds}, and b_w are the viscous frictions of the propeller, the final drive and the wheels, respectively. k_{ps} and k_{ds} are the propeller position and the final drive position coefficients, respectively [17].

Longitudinal Vehicle Motion

Based on Newton's second law, the total force acting on a vehicle while moving in a longitudinal direction is:

$$F_t(t) - F_a(t) - \sum F_{rt}(t) = 0$$

The traction force:

$$F_t(t) = \frac{T_w(t)}{r_w}$$

The acceleration force:

$$F_a(t) = \left(m_v r_w n + J_{eq}\right)\frac{d\omega_m(t)}{dt}$$

The total resistance force:

$$\sum F_{rt}(t) = F_d(t) + F_g(t) + F_{Rx}(t) + F_{tk}(t)$$

The wind drag force:

$$F_d(t) = K_d v_v^2$$

The gradient force is

$$F_g(t) = m_v g \sin\theta$$

The rolling resistance force:

$$F_{Rx}(t) = m_v g C_{Rx}\cos\theta$$

The curvature resistance force:

$$F_{tk}(t) = m_v g\left(\frac{k_{tk}}{R}\right)$$

The total equivalent moment inertia in Equation (9) is given by:

$$J_{tot} = \left(m_v r_w n + J_{eq}\right) r_w$$

with $K_d = \frac{1}{2}\rho C_d A_f$; m_v is the vehicle mass, r_w is the wheel radius, ρ is the air density, C_d is the wind drag coefficient, A_f is the area frontal, C_{Rx} is the rolling coefficient, g is the gravity constant, θ is the gradient, k_{tk} is the curvature constant and R is the curvature distance [8], [18], [19].

APPENDIX B
DYNAMICAL EQUATIONS OF MODELS

A general model can be expressed in state space equation as following i.e. SMK-1, SMK-2, IMK-1, IMK-2, IMK-3 and IMK-4.

SMK-1: Simple Model with Rigid Shaft

$$\frac{di_m(t)}{dt} = -\frac{k_e}{L_m}\omega_m(t) - \frac{R_m}{L_m}i_m(t) + \frac{1}{L_m}u_c(t)$$

$$\frac{d\omega_m(t)}{dt} = -\frac{b_{eq}r_w}{J_{tot}}\omega_m(t) + \frac{k_t}{nJ_{tot}}i_m(t)$$

$$- \frac{1}{J_{tot}}m_v g r_w\left(\sin\theta + C_{Rx}\cos\theta + \frac{k_{tk}}{R}\right)$$

SMK-2: Simple Model with Flexible Shaft

$$\frac{di_m(t)}{dt} = -\frac{k_e}{L_m}\omega_m(t) - \frac{R_m}{L_m}i_m(t) + \frac{1}{L_m}u_c(t)$$

$$\frac{d\omega_w(t)}{dt} = \frac{k_t}{nJ_{f2}}i_m(t) - \frac{b_{f2}}{J_{f2}}\omega_w(t) - \frac{k_{ds}r_w}{J_{f2}}\theta_w(t)$$

$$+ \frac{b_{ds}r_w}{J_{f2}}\omega_d(t) + \frac{k_{ds}r_w}{J_{f2}}\theta_d(t)$$

$$- \frac{m_v g r_w}{J_{f2}}\left(\sin\theta + C_{Rx}\cos\theta + \frac{k_{tk}}{R}\right)$$

$$\frac{d\theta_m(t)}{dt} = \omega_m(t)$$

$$\frac{d\theta_d(t)}{dt} = \omega_d(t)$$

$$\frac{d\theta_w(t)}{dt} = \omega_w(t)$$

IMK-1: IBEV Model with Rigid Shaft & Lithium-ion

$$\frac{di_m(t)}{dt} = -\frac{k_e}{L_m}\omega_m(t) - \frac{R_m}{L_m}i_m(t) + \frac{1}{L_m}\left(-R_d i_m(t)\right.$$

$$\left. - V_{c1}(t) - V_{c2}(t) + 2a_1 SOC_n(t)\right.$$

$$\left. + (2a_1 + 2a_0))K_c u_c(t)\right.$$

$$\frac{d\omega_m(t)}{dt} = -\frac{b_{eq}r_w}{J_{tot}}\omega_m(t) + \frac{k_t}{nJ_{tot}}i_m(t) - n^2 K_d r_w^3 \omega_m^2$$

$$- \frac{1}{J_{tot}}m_v g r_w\left(\sin\theta + C_{Rx}\cos\theta + \frac{k_{tk}}{R}\right)$$

$$\frac{dV_{c1}(t)}{dt} = -\frac{1}{R_{t1}C_{t1}}V_{c1}(t) + \frac{1}{C_{t1}}i_b(t)$$

$$\frac{dV_{c2}(t)}{dt} = -\frac{1}{R_{t2}C_{t2}}V_{c2}(t) + \frac{1}{C_{t2}}i_b(t)$$

$$\frac{dSOC_n(t)}{dt} = -\frac{1}{Q_n}i_b(t).$$

IMK-3: IBEV Model with Flexible Shaft & Lithium ion

$$\frac{di_m(t)}{dt} = -\frac{k_e}{L_m}\omega_m(t) - \frac{R_m}{L_m}i_m(t)$$

$$+ \frac{1}{L_m}\left(-R_d i_m(t) - V_{c1}(t) - V_{c2}(t)\right.$$

$$\left. + 2a_1 SOC_n(t) + (2a_1 + 2a_0))K_c u_c(t)\right.$$

$$\frac{d\omega_m(t)}{dt} = \frac{k_t}{J_{f1}}i_m(t) - \frac{b_{f1}}{J_{f1}}\omega_m(t) - \frac{1}{n_g^2 J_{f1}}k_{ps}\theta_m(t)$$

$$+ \frac{n_t}{n_g J_{f1}} b_{ps} \omega_d(t) + \frac{n_t}{n_g J_{f1}} k_{ps} \theta_d(t)$$

$$\frac{d\omega_d(t)}{dt} = -\frac{b_{ds}}{J_{ds}} \omega_d(t) + \frac{b_{ds}}{J_{ds}} \omega_w(t) - \frac{k_{ds}}{J_{ds}} \theta_d(t) + \frac{k_{ds}}{J_{ds}} \theta_w(t)$$

$$\frac{d\omega_w(t)}{dt} = \frac{k_t}{n J_{f2}} i_m(t) - \frac{b_{f2}}{J_{f2}} \omega_w(t) - \frac{k_{ds} r_w}{J_{f2}} \theta_w(t)$$
$$+ \frac{b_{ds} r_w}{J_{f2}} \omega_d(t) + \frac{k_{ds} r_w}{J_{f2}} \theta_d(t) - \frac{1}{J_{f2}} K_d r_w^3 \omega_w(t)^2$$
$$- \frac{m_v g r_w}{J_{f2}} \left(sin\,\theta + C_{Rx} cos\,\theta + \frac{k_{tk}}{R} \right)$$

$$\frac{d\theta_m(t)}{dt} = \omega_m(t), \quad \frac{d\theta_d(t)}{dt} = \omega_d(t), \quad \frac{d\theta_w(t)}{dt} = \omega_w(t)$$

$$\frac{dV_{c1}(t)}{dt} = -\frac{1}{R_{t1} C_{t1}} V_{c1}(t) + \frac{1}{C_{t1}} i_b(t)$$

$$\frac{dV_{c2}(t)}{dt} = -\frac{1}{R_{t2} C_{t2}} V_{c2}(t) + \frac{1}{C_{t2}} i_b(t)$$

$$\frac{dSOC_n(t)}{dt} = -\frac{1}{Q_n} i_b(t)$$

IMK-2 IBEV Model with Rigid Shaft & Lead acid

$$\frac{di_m(t)}{dt} = -\frac{k_e}{L_m} \omega_m(t) - \frac{R_m}{L_m} i_m(t)$$
$$+ \frac{1}{L_m} (E_{mb0} - R_{00} i_m(t) + (273 k_1$$
$$+ k_1 \theta_b(t) - k_2 i_1(t) + k_3 i_m(t)) Q_b(t)) K_c u_c(t)$$

$$\frac{d\omega_m(t)}{dt} = -\frac{b_{eq} r_w}{J_{tot}} \omega_m(t) + \frac{k_t}{n J_{tot}} i_m(t) - n^2 K_d r_w^3 \omega_m^2$$
$$- \frac{1}{J_{tot}} m_v g r_w \left(sin\,\theta + C_{Rx} cos\,\theta + \frac{k_{tk}}{R} \right)$$

$$\frac{d\theta_b(t)}{dt} = \frac{R_{02}}{C_{\theta b}} i_b(t)^2 - \frac{1}{R_{\theta b} C_{\theta b}} \theta_b(t) + \frac{\theta_{\alpha b}}{R_{\theta b} C_{\theta b}}$$

$$\frac{dQ_b(t)}{dt} = i_b(t)$$

$$\frac{di_1(t)}{dt} = \frac{1}{k_2 C_1 Q_b(t)} (i_b(t) + i_1(t))$$

IMK-4: IBEV Model with Flexible Shaft & Lead acid

$$\frac{di_m(t)}{dt} = -\frac{k_e}{L_m} \omega_m(t) - \frac{R_m}{L_m} i_m(t)$$
$$+ \frac{1}{L_m} (E_{mb0} - R_{00} i_m(t) + (273 k_1 + k_1 \theta_b(t)$$
$$- k_2 i_1(t) + k_3 i_m(t)) Q_b(t)) K_c u_c(t)$$

$$\frac{d\omega_m(t)}{dt} = \frac{k_t}{J_{f1}} i_m(t) - \frac{b_{f1}}{J_{f1}} \omega_m(t) - \frac{1}{n_g^2 J_{f1}} k_{ps} \theta_m(t)$$
$$+ \frac{n_t}{n_g J_{f1}} b_{ps} \omega_d(t) + \frac{n_t}{n_g J_{f1}} k_{ps} \theta_d(t)$$

$$\frac{d\omega_d(t)}{dt} = -\frac{b_{ds}}{J_{ds}} \omega_d(t) + \frac{b_{ds}}{J_{ds}} \omega_w(t) - \frac{k_{ds}}{J_{ds}} \theta_d(t) + \frac{k_{ds}}{J_{ds}} \theta_w(t)$$

$$\frac{d\omega_w(t)}{dt} = \frac{k_t}{n J_{f2}} i_m(t) - \frac{b_{f2}}{J_{f2}} \omega_w(t) - \frac{k_{ds} r_w}{J_{f2}} \theta_w(t)$$
$$+ \frac{b_{ds} r_w}{J_{f2}} \omega_d(t) + \frac{k_{ds} r_w}{J_{f2}} \theta_d(t) - \frac{1}{J_{f2}} K_d r_w^2 \omega_w(t)^2$$
$$- \frac{m_v g r_w}{J_{f2}} \left(sin\,\theta + C_{Rx} cos\,\theta + \frac{k_{tk}}{R} \right)$$

$$\frac{d\theta_m(t)}{dt} = \omega_m(t), \quad \frac{d\theta_d(t)}{dt} = \omega_d(t), \quad \frac{d\theta_w(t)}{dt} = \omega_w(t)$$

$$\frac{d\theta_b(t)}{dt} = \frac{R_{02}}{C_{\theta b}} i_b(t)^2 - \frac{1}{R_{\theta b} C_{\theta b}} \theta_b(t) + \frac{\theta_{\alpha b}}{R_{\theta b} C_{\theta b}}$$

$$\frac{dQ_b(t)}{dt} = i_b(t)$$

$$\frac{di_1(t)}{dt} = \frac{1}{k_2 C_1 Q_b(t)} (i_b(t) + i_1(t))$$

REFERENCES

[1] A. G. Boulanger, A. C. Chu, S. Maxx, and D. L. Waltz, "Vehicle electrification: Status and issues," *Proc. IEEE*, vol. 99, no. 6, pp. 1116–1138, Jun. 2011.

[2] T. Schwicarkt, H. Voos, J.-R. Hadji-Minaglou, M. Darouach, and A. Rosich, "Design and simulation of a real-time implementable energy-efficient model-predictive cruise controller for electric vehicles," *J. Franklin Inst.*, vol. 352, no. 2, pp. 603–625, Feb. 2015.

[3] Q. Yan, B. Zhang, and M. Kezunovic, "Optimization of electric vehicle movement for efficient energy consumption," in *Proc. IEEE Proc. North Amer. Power Symp. (NAPS)*, Pulman, WA, USA, Sep. 2014, pp. 1–6.

[4] X. Wu, X. He, G. Yu, A. Harmandayan, and Y. Wang, "Energy-optimal speed control for electric vehicles on signalized arterials," *IEEE Trans. Intell. Transp. Syst.*, vol. 16, no. 5, pp. 2786–2796, Oct. 2015.

[5] X. Huang and J. Wang, "Nonlinear model predictive control for improving energy recovery for electric vehicles during regenerative braking," in *Proc. 50th IEEE Conf. Decis. Control Eur. Control Conf. (CDC-ECC)*, Orlando, FL, USA, Dec. 2011, pp. 7458–7463.

[6] W. Dib, L. Serrao, and A. Sciarretta, "Optimal control to minimize trip time and energy consumption in electric vehicles," in *Proc. IEEE Vehicle Power Propuls. Conf. (VPPC)*, Chicago, IL, USA, Sep. 2011, pp. 1–8.

[7] P. Sauter, M. Flad, and S. Hohmann, "Subliminal optimal longitudinal vehicle control for energy efficient driving," in *Proc. IEEE Int. Conf. Syst., Man Cybern. (SMC)*, San Diego, CA, USA, Oct. 2014, pp. 3001–3007.

[8] T. D. Gillespie, *Fundamentals of Vehicle Dynamics*. Warrendale, PA, USA: Society of Automotive Engineers, 1992.

[9] G. L. Plett. (2014). *Battery Modelling, Simulation and Identification of Battery Dynamics*. [Online]. Available: http://www.apple.com/quicktime/download/.

[10] M. Oswal, J. Paul and R. Zhao, "A comparative study of lithium ion batteries," Univ. Southern California, Los Angeles, CA, USA, 2010.

[11] W. Peng, "Accurate circuits model for predicty the performance of lead acid AGM batteries," M.S. thesis, Dept. Elect. Comput. Eng., Univ. Nevada, Reno, NV, USA, 2011.

[12] R. A. Jackey, *A Simple, Effective Lead-Acid Battery Modeling Process for Electrical System Component Selection*. Natick, MA, USA: Mathworks Inc., 2007.

[13] S. Barsali and M. Ceraolo, "Dynamical models of lead-acid batteries: Implementation issues," *IEEE Trans. Energy Convers.*, vol. 17, no. 1, pp. 16–23, Mar. 2002.

[14] S. Rambambu, "Modeling and control of a brushless DC motor," M.S. thesis, Dept. Elect. Eng., Nat. Inst. Technol., Rourkela, India, 2017.

[15] Y. Haroen, "Kontribusi analisis induktansi sendiri dan induktansi bersama pada sirkuit listrik dan mesin listrik arus bolak balik 3 Fasa," *J. Math. Fundam. Sci.*, vol. 27, no. 2, pp. 1–27, 1994.

[16] K. Ogata, *Modern Control Engineering*, 4th ed. Upper Saddle River, NJ, USA: Prentice-Hall, 2002.

[17] O. Sato, H. Shimojima, and T. Kaneko, "Positioning control of a gear train system including flexible shafts," *JSME Int. J.*, vol. 30, no. 267, pp. 1465–1472, Sep. 1987.

[18] M. Raffaele, "Modelling and simulation of the dynamic behavior of the automobile," M.S. thesis, Fac. Eng., Univ. degli studi di salerno, Fisciano, Italy, 2012.

[19] Y. Haroen, *Sistem Transportasi Elektrik*. Bandung, Indonesia: ITB Press, 2012.

[20] R. Ristiana, A. S. Rohman, A. Purwadi, H. Hindersah, C. Machbub, and E. Rijanto, "Torque control using integrated battery-electric vehicle model with flexible shaft," in *Proc. Int. Conf. Electr. Veh. Technol. (ICEVT)*, Sanur, Indonesia, Oct. 2017, pp. 24–29.

[21] R. Ristiana, A. S. Rohman, A. Purwadi, E. Rijanto, and C. Machbub, "Energy efficient speed control using IBEV model in an EV testbed platform," in *Proc. IEEE Int. Conf. Syst. Eng. Technol. (ICSET)*, Bandung, Indonesia, Oct. 2018, pp. 46–50.

[22] *Mathwork*. Accessed: Sep. 25, 2016. [Online]. Available: https://www.mathworks.com

[23] R. Ristiana, A. Syaichu-Rohman, E. Rijanto, A. Purwadi, and C. Machbub, "Designing optimal speed control with observer using integrated battery-electric vehicle (IBEV) model for energy efficiency," *J. Mechatronics, Elect. Power, Veh. Technol.*, vol. 9, no. 2, pp. 89–100, Dec. 2018.

[24] R. M. Murray, "Optimization-based control," California Inst. Technol., Pasadena, CA, USA, 2009, pp. 111–128.

[25] R. Ristiana, A. S. Rohman, A. Purwadi, and C. Machbub, "Integrated battery-electric vehicle model and its optimal speed control application," in *Proc. 3rd Int. Conf. Control, Automat. Robot. (ICCAR)*, Nagoya, Japan, Apr. 2017, pp. 588–592.

[26] R. Ristiana, A. Syaichu-Rohman, A. Purwadi, and C. Machbub, "Energy efficient torque control using integrated battery-electric vehicle model," in *Proc. Int. Conf. Syst. Eng. Technol. (ICSET)*, Shah Alam, Malaysia, Oct. 2017, pp. 223–228.

[27] R. Ristiana, A. S. Rohman, A. Purwadi, H. E. Hindersah Rijanto, and C. Machbub, "Implementation IBEV model and its speed control applications in Molina ITB for energy efficiency," in *Proc. IEEE Int. Conf. Electr. Veh. Technol. (ICEVT)*, Solo Indonesia, Oct. 2018, pp. 68–71.

RINA RISTIANA was born in Bandung. She graduated from the Faculty of Electrical Engineering, Universitas Islam Nusantara, Bandung, in 2000, and the M.E. degree in control and intelligent system (electrical engineering) from the School of Electrical Engineering and Informatics, Institut Teknologi Bandung (ITB), in 2013. She is currently pursuing the Ph.D. degree with the School of Electrical Engineering and Informatics, Institut Teknologi Bandung (ITB). Since 2006, she has been with the Indonesian Institute of Sciences as an Engineering Researcher. Her research interests include automation and control instrumentation process equipment and electrical machines and drives, and electric transportation.

ARIEF SYAICHU ROHMAN was born in Malang, East Java, Indonesia. He received the bachelor's (Ir.) degree in electrical engineering from the Institut Teknologi Bandung (ITB), Indonesia, in 1990, the M.Eng.Sc. degree in systems and control from the University of New South Wales, Sydney, Australia, in 1998, and the Ph.D. degree in systems and control from the University of Newcastle, Newcastle, Australia, in 2005. He was with the Research and Development Division, PT IPTN, the Indonesian Aircraft Industry, from 1990 to 1992. He has been teaching undergraduate and graduate courses in electrical engineering with the School of Electrical Engineering and Informatics, ITB, Indonesia, since 1992. He served as the Head of the Undergraduate Program in Electrical Engineering, School of Electrical Engineering and Informatics, ITB, for four years from 2012. He has published papers in various national and international journals and conferences. His research interests include anti-windup systems, model predictive control, sliding-mode control and their applications including distillation column, electric vehicle, and auto drive systems.

CARMADI MACHBUB received the bachelor's degree in electrical engineering from the Institut Teknologi Bandung (ITB), in 1980, and the master's degree (DEA) in control engineering and industrial informatics and the Ph.D. degree in engineering sciences majoring in control engineering and industrial informatics from Ecole Centrale de Nantes, in 1988 and 1991, respectively. He is currently a Professor and the Head of the Control and Computer Systems Research Division, School of Electrical Engineering and Informatics, ITB. His current research interests include machine perception, optimization, and control.

AGUS PURWADI was born in Jakarta, in August 1957. He received the bachelor's, master's, and Ph.D. degrees in electrical power engineering from the Department of Electrical Engineering, Institut Teknologi Bandung (ITB), in 1985, 2004, and 2010, respectively. Since 1987, he has been a Lecturer with the Department of Electrical Engineering, School of Electrical Engineering and Informatics, ITB. From 2012 to 2015, he was the Head of the Technical Team, National Electric Vehicle Research and Development Program, Ministry of Research, Technology and Higher Education. Since 2015, he has also been the Head of the Electrical Energy Conversion Research Laboratory, ITB. Since 2017, he has also been a Researcher with the National Centre for Sustainable Transportation Technology, ITB. He holds National Registered Patent on 30 kW BLDC motor for EV-City Car. His research interests include electrical machines and drives, electric transportation, renewable energy technology, and smart grid systems. He is a member of the Indonesian Association of Engineers-PII, the IEEE-PES Society, and the IEEE-VTS Society.

ESTIKO RIJANTO was born in Purbalingga, Indonesia, in 1967. He received the B.Eng. degree in mechanical systems engineering and the M.Eng. and Dr.Eng. degrees from the Tokyo University of Agriculture and Technology (TUAT), Tokyo, Japan, in 1993, 1995, and 1998, respectively. He was granted a postdoctoral program at the Venture Business Laboratory TUAT-Tokyo, where he completed his book on Robust Control. He continued his postdoctoral program at NSK Company Ltd., Maebashi, Japan, where he served as a Project Engineer for the development of electric power steering control systems for city cars. Since 2002, he has been conducting Research and Development activities at the Research Center for Electrical Power and Mechatronics, Indonesian Institute of Sciences (LIPI), Bandung, Indonesia. Since 2011, he has also been serving as a Consultant for the state-owned electricity company in the development and implementation of digital electro-hydraulic govenor and excitation systems for coal-fired, geothermal, and hydropower plants. In 2013, he was inaugurated the Research Professor on Applied Control Systems by LIPI. His research interests include control systems and their applications for power generations, power electronics, renewable energies, battery management systems, electric vehicles, robotics, and mechatronics.

● ● ●